american physiological society

JNP JOURNAL OF NEUROPHYSIOLOGY

J Neurophysiol 129: 1127–1144, 2023.
First published April 19, 2023; doi:10.1152/jn.00498.2022

RESEARCH ARTICLE

Neural Circuits

Spike timing-dependent plasticity alters electrosensory neuron synaptic strength in vitro but does not consistently predict changes in sensory tuning in vivo

Adalee J. Lube, Xiaofeng Ma, and Bruce A. Carlson

Department of Biology, Washington University in St. Louis, St. Louis, Missouri, United States

Abstract

How do sensory systems optimize detection of behaviorally relevant stimuli when the sensory environment is constantly changing? We addressed the role of spike timing-dependent plasticity (STDP) in driving changes in synaptic strength in a sensory pathway and whether those changes in synaptic strength could alter sensory tuning. It is challenging to precisely control temporal patterns of synaptic activity in vivo and replicate those patterns in vitro in behaviorally relevant ways. This makes it difficult to make connections between STDP-induced changes in synaptic physiology and plasticity in sensory systems. Using the mormyrid species *Brevimyrus niger* and *Brienomyrus brachyistius*, which produce electric organ discharges for electrolocation and communication, we can precisely control the timing of synaptic input in vivo and replicate these same temporal patterns of synaptic input in vitro. In central electrosensory neurons in the electric communication pathway, using whole cell intracellular recordings in vitro, we paired presynaptic input with postsynaptic spiking at different delays. Using whole cell intracellular recordings in awake, behaving fish, we paired sensory stimulation with postsynaptic spiking using the same delays. We found that Hebbian STDP predictably alters sensory tuning in vitro and is mediated by NMDA receptors. However, the change in synaptic responses induced by sensory stimulation in vivo did not adhere to the direction predicted by the STDP observed in vitro. Further analysis suggests that this difference is influenced by polysynaptic activity, including inhibitory interneurons. Our findings suggest that STDP rules operating at identified synapses may not drive predictable changes in sensory responses at the circuit level.

NEW & NOTEWORTHY We replicated behaviorally relevant temporal patterns of synaptic activity in vitro and used the same patterns during sensory stimulation in vivo. There was a Hebbian spike timing-dependent plasticity (STDP) pattern in vitro, but sensory responses in vivo did not shift according to STDP predictions. Analysis suggests that this disparity is influenced by differences in polysynaptic activity, including inhibitory interneurons. These results suggest that STDP rules at synapses in vitro do not necessarily apply to circuits in vivo.

Hebbian plasticity; sensory processing; synaptic plasticity; temporal coding; weakly electric fish

INTRODUCTION

How does a sensory system optimize detection of behaviorally relevant stimuli amid constant changes in those stimuli and to the sensory environment? To efficiently process sensory information, sensory systems are tuned to specific stimulus attributes. Rather than being tuned to every possible stimulus variant, a more efficient approach is for the neuronal tuning of a sensory system to adapt to changing stimulus statistics. Sensory systems are known to adapt to a variety of complex stimulus statistics, such as the probability of occurrence in the environment, stimulus rate, stimulus distribution, local stimulus mean, variation in stimulus statistics, intensity, and more (1, 2). For example, retinal ganglion cells adjust their firing rate two- to fivefold in response to changes in image contrast, providing a mechanism for contrast adaptation (3). In guinea pig auditory midbrain, the neuronal population as a whole shifts their responses to best encode commonly occurring sounds, though the mechanism for this shift remains unknown (4). Electrosensory pyramidal neurons in gymnotiform weakly electric fish respond maximally to low frequencies under local spatial stimulation, whereas

Correspondence: B. A. Carlson (carlson.bruce@wustl.edu).
Submitted 12 December 2022 / Revised 12 April 2023 / Accepted 13 April 2023

they respond maximally to high frequencies under more global stimulation (5). This may be due to different amounts of inhibitory input in these different stimulus contexts. A variety of examples exist showing shifts in neuronal tuning depending on behavioral context (2, 6–8), but are there common mechanisms that could allow for tuning adaptation in a quickly changing sensory environment?

The adjustment of synaptic connectivity via spike timing-dependent plasticity (STDP), wherein synaptic strength is altered based on the relative timing of repetitive pre- and postsynaptic activity, is known to alter neuronal responses in sensory circuits across diverse invertebrate and vertebrate organisms (9–13). For example, STDP is involved in the development of receptive fields (14, 15) and establishment of direction selectivity within the visual system (16) and in the adult function of many circuits, including in humans (17–19). However, it remains unclear whether STDP is a mechanism for altering sensory tuning in adult organisms in real time.

Mormyrid weakly electric fish produce and receive electric organ discharges (EODs) that they use to electrolocate and communicate. EODs have two salient features: waveform, which signals sender identity, and interpulse interval (IPI), which signals contextual information (20). Mormyrids have a sensory pathway dedicated to processing electric communication signals (Fig. 1) (21, 22). The waveform of each EOD is encoded into spike timing differences among peripheral electroreceptors called knollenorgans (KOs), whereas interspike intervals within KOs encode IPIs (21). The KO afferent fibers project to the nucleus of the electrosensory lateral line lobe in the hindbrain, where corollary discharge inhibition blocks responses to the fish's own EOD but not to external EODs generated by other fish (23). This timing information is relayed to the midbrain anterior exterolateral nucleus (ELa), where EOD waveform tuning originates (24, 25). ELa provides topographic, excitatory input to the posterior exterolateral nucleus (ELp) (24), where single-neuron IPI tuning is established (26). Because ELa output precisely follows the timing of electric stimulus pulses (25), we can stimulate ELp in vitro and in vivo with the exact same temporal patterns. This allows us to have precise control of the timing of presynaptic input using behaviorally relevant stimuli in vivo and to replicate those temporal patterns in vitro.

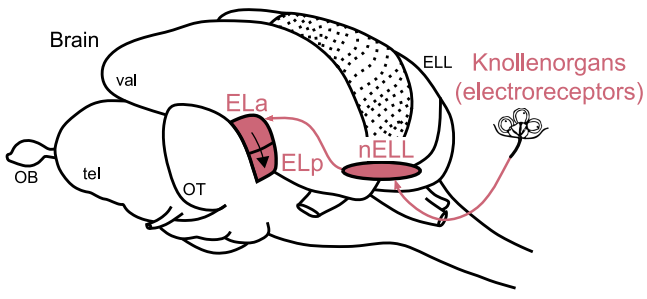

Figure 1. The mormyrid knollenorgan sensory pathway mediates electric communication behavior. Electric organ discharge (EOD) stimuli are detected by knollenorgan electroreceptors. Each knollenorgan responds to each EOD with a single spike. The timing of these spikes varies across the population with variation in EOD waveform. Thus, EOD waveforms are represented by spike timing differences and interpulse intervals (IPIs) are represented by interspike interval sequences. This information is relayed to the nucleus (nELL) of the electrosensory lateral line lobe (ELL). Inhibition from this pathway blocks responses to the fish's own EOD. From the nELL, information is sent to the anterior exterolateral nucleus (ELa), which is tuned to EOD waveform. The ELa projects to the posterior exterolateral nucleus (ELp). The integration of synaptic inputs from ELa and local excitatory and inhibitory interactions among ELp neurons establishes single-neuron tuning for both EOD waveform and IPI. OB, olfactory bulb; OT, optic tectum; tel, telencephalon; val, valvula.

Indeed, ELp multipolar cells show the same IPI tuning in response to direct ELa stimulation in vivo as they do to sensory stimulation (26). Within the ELp, excitatory and inhibitory multipolar neurons shape tuning to EOD waveform and IPI (21). Excitatory multipolar cells form extensive interconnections with each other (27). They are more likely to share an excitatory connection with cells having similar IPI tuning, and connections between cells with similar IPI tuning are stronger than connections between cells with dissimilar tuning (27). In addition, local excitatory connections between ELp multipolar cells are more common at short distances (27). The dense interconnections among these timing-sensitive cells and the temporal precision of afferent input to ELp motivated experiments to test whether STDP affects the topology of this network.

In addition, we have access to two species, *Brevimyrus niger and Brienomyrus brachyistius,* that are distantly related members of clade A (28). Previous comparative work has shown that the cellular anatomy and physiology of ELp is similar across clade A species (28, 29). Studying these two distantly related species allows us to ask whether STDP is a common mechanism operating in ELp neurons across clade A species.

In the present study, we show that STDP can alter the synaptic responses of ELp neurons in vitro, but these changes did not reliably predict changes in sensory tuning in vivo. Analysis of variation in synaptic responses suggests that differences in local connectivity in vivo relative to in vitro affect the direction of synaptic changes induced by STDP.

MATERIALS AND METHODS

Animals

In this study, we used a total of 95 *B. niger* of both sexes, ranging from 4.5 to 9.4 cm in standard length and from 0.8 to 13.5 g in mass, and 40 *B. brachyistius* of both sexes, ranging from 6.6 to 10 cm in standard length and from 4.2 to 20.1 g in mass. We acquired the fish through the aquarium trade and housed them in same-species groups with a 12:12-h light-dark cycle, water conductivity of 200–400 μS/cm, and a temperature of 25–29°C. We fed the fish live black worms four times per week. All procedures were in accordance with the guidelines established by the National Institutes of Health and were approved by the Institutional Animal Care and Use Committee at Washington University in St. Louis. *B. brachyistius* were used for the *B. brachyistius*-specific experiment in vitro and for the EOD tuning experiments in vivo; otherwise *B. niger* were used.

In Vitro Whole Brain Preparation

We used an in vitro whole brain preparation and recording method used in previous studies (27, 30). We anesthetized fish in 300 mg/L tricaine methanesulfonate (MS-222) and then submerged fish in ice-cold, oxygenated artificial

cerebrospinal fluid (ACSF; composition in mM: 124 NaCl, 2.0 KCl, 1.25 KH_2PO_4, 24 $NaHCO_3$, 2.6 $CaCl_2$, 1.6 $MgSO_4{\cdot}7H_2O$, and 20 glucose, pH 7.2–7.4; osmolarity 300–305 mosM) before performing a craniotomy to fully expose the brain. While the brain remained submerged, all cranial nerves were cut, the connection to the spinal cord was severed, and the valvula cerebellum was removed by suction, leaving the remaining hindbrain, midbrain, and forebrain intact. The brain was then removed and placed in an incubating chamber containing oxygenated ACSF at 29°C for 1 h. The brain was then transferred to a recording chamber (Warner Instruments RC-26GLP) that was continuously perfused with oxygenated ACSF at room temperature (flow rate = 1 mL/min), where it was placed on an elevated slice hold-down with a 1.0-mm mesh size (Warner Instruments SHD-26GH/10). A second slice hold-down with a 1.5-mm mesh size (Warner Instruments SHD-26GH/15) was placed on top of the brain, and it was held securely in place with cured silicone placed at the top of the chamber. Some of the threads of the upper hold-down were cut to improve access to the ELa and the ELp. This configuration helped keep the preparation stable while also maximizing tissue survival by allowing a constant flow of oxygenated ACSF both beneath and above the preparation.

In Vitro Whole Cell Recording

We visualized ELp neurons with transmitted light in an upright fixed-stage microscope (BX51WI; Olympus) and a Newvicon tube camera (Dage-MTI). We obtained whole cell intracellular recordings with filamented borosilicate patch pipettes (1.00-mm outer diameter; 0.58-mm inner diameter) with tip resistances of 6.2–10.2 MΩ as described previously (31). The electrode internal solution contained the following (in mM): 130 K gluconate, 5 EGTA, 10 HEPES, 3 KCl, 2 $MgCl_2$, 4 Na_2ATP, 5 Na_2 phosphocreatine, and 0.4 Na_2GTP, pH 7.3–7.4 (osmolarity: 285–290 mosM). Electrodes were mounted in a headstage (Molecular Devices CV-7B), which was connected to a multichannel amplifier (Molecular Devices MultiClamp 700B) for current-clamp recording. Data were digitized at a sampling rate of 50 kHz (Molecular Devices Digidata 1440A) and saved to disk (Molecular Devices Clampex v10.2). The position of the electrode was controlled by a manipulator (Sutter Instruments MP-285) connected to a controller (Sutter Instruments MPC-200 and ROE-200). Healthy ELp neurons were identified on the basis of location and a relatively low-contrast, round somatic boundary. We targeted somas of all possible sizes and locations throughout ELp within ~20–50 μm of the surface, depending on tissue thickness. Seal resistance varied from 1.3 to 4.8 GΩ, and input resistance varied from 230 to 290 MΩ. We only used data from neurons that had stable access and input resistances and a stable resting potential of at least −50 mV.

In Vitro Data Collection

For focal presynaptic stimulation, we placed a glass stimulus electrode in ELa, just anterior to the ELp border, and another in the solution just above the brain as a reference electrode. We delivered biphasic, square current pulses with a total duration of 100 μs and amplitudes ranging from 50 to 200 μA through pulse generators (A-M Systems model 2100) triggered by a single digital output (Molecular Devices Digidata 1440A). Stimulus amplitude was adjusted to yield reliable, subthreshold postsynaptic potentials from the recorded neuron. Five synaptic potentials evoked by ELa stimulation were averaged to measure the amplitude of excitatory postsynaptic potentials (EPSPs). We defined the resting potential as the average membrane potential within a 50-ms window during the prestimulus period.

Experiments were also done with an array of stimulus electrodes for presynaptic stimulation rather than a single glass stimulus electrode. The array consisted of four channels of bipolar stimulation (8 electrodes total), in the form of either a "cluster" electrode (FHC model CE) or a "matrix" electrode (FHC model MX). We placed this array in ELa, just anterior to the ELp border. The rest of the stimulus protocol described above for the focal glass stimulus electrode was the same for the array stimulus electrodes.

For STDP induction, each EPSP induced by ELa stimulation was paired with a spike evoked by a 2-ms depolarizing 600-μA pulse injected via the patch pipette, which was sufficient to induce an action potential in the postsynaptic neuron. In *B. niger*, we paired EPSPs and spikes at −80-, −50-, −40-, −30-, −20-, −10-, −5-, 0-, +5-, +10-, +20-, +30-, +40-, +50-, and +80-ms pre-post delays. We randomly chose the pairing delay that each neuron was subjected to. There were three controls: ELa stimulation only, intracellular stimulation only, and no stimulation. All pairings and ELa stimulation-only and intracellular stimulation-only control conditions were repeated at 1 Hz for 6 min. The no-stimulation control lasted 6 min. In *B. brachyistius*, we only paired EPSPs and spikes at −20- and +10-ms pre-post delays, with no controls. After EPSP-spike pairing, the EPSP evoked by ELa stimulation was recorded again (repeated 5 times and averaged) to compare with the baseline, prepairing EPSP. To measure the max of the PSP, we found the maximum point in a window from the end of the stimulus to 200 ms. In this same window, to measure the PSP area over time, we summed the poststimulus synaptic potential trace and multiplied by 1 over the sampling frequency (1/sampling frequency = sampling period).

To test the role of STDP in shaping IPI tuning, we paired IPI trains of ELa stimulation with intracellular spiking. We delivered two trains of ELa stimulation: the first train consisted of 10 pulses at 10-ms IPI, and the second train consisted of 10 pulses at 100-ms IPI. Both IPI trains were repeated 30 times to get an averaged postsynaptic potential baseline response. During pairing, we delivered the 10-ms IPI train, followed by 450 ms of silence, and then the 100-ms IPI train. While this ELa stimulation was delivered, either the 10-ms IPI train or the 100-ms IPI train was paired with 10 pulses of 10-ms IPI or 100-ms IPI postsynaptic spikes evoked by 600-μA current injection via the patch pipette with a −20-ms pre-post delay. This pairing was repeated 300 times. Both IPI trains were then repeated 30 times to get an averaged postsynaptic potential response after pairing. We measured the maximum depolarization in response to each stimulus pulse relative to rest and then averaged the maximum depolarizations in response to the 2nd through 10th pulses to quantify the response to each IPI. To measure the

PSP area over time, in a window from the end of the first stimulus in the IPI train to the start of the second stimulus in the IPI train we summed the poststimulus synaptic potential trace and multiplied by 1 over the sampling frequency (1/sampling frequency = sampling period).

In Vitro Pharmacology

To assess the role of NMDA versus non-NMDA receptors in mediating STDP, we bath applied the NMDA receptor antagonist DL-2-amino-5-phosphonopentanoic acid (APV; Tocris 0105) or the non-NMDA receptor antagonist 6,7-dinitroquinoxaline-2,3-dione (DNQX; Tocris 2312). Both drugs were delivered at a concentration of 50 μM in ACSF. Full washout typically took 15–20 min. During bath application, EPSPs evoked by ELa stimulation were paired with a spike evoked by a 2-ms depolarizing 600-μA pulse injected via the patch pipette. We paired EPSPs and spikes for 6 min at 1 Hz with delays at −20 ms and +10 ms (pre-post). We randomized the sequence in which the delays were paired. After EPSP-spike pairing, EPSPs evoked by ELa stimulation were recorded again (repeated 5 times and averaged) to compare with the baseline EPSP.

In Vivo Whole Cell Recordings

We prepared fish for in vivo recordings from ELp as described previously (26, 32). Fish were anesthetized in 300 mg/L tricaine methanesulfonate (MS-222) and paralyzed with an intramuscular injection of 100 μL of 0.1 mg/mL gallamine triethiodide (Flaxedil). The fish was then moved to a recording chamber, where it was submerged in freshwater, except for a small region of the surface of the head. We maintained general anesthesia for surgery by respirating the fish with an aerated solution of 100 mg/mL MS-222 through a pipette tip in the mouth. The surgery site was anesthetized with 0.4% lidocaine on the skin. We then removed the skin of the surgery site, affixed a post to the skull, and removed a rectangular piece of skull covering ELp. We placed the ground electrode on the nearby cerebellum. After surgery, we brought the fish out of anesthesia by switching to aerated freshwater respiration and monitored the fish's electric organ discharge command (EODC) output with a pair of electrodes placed next to the fish's tail (20, 26, 32, 33). The EOD output is silenced by Flaxedil (the muscle paralytic), but we recorded the EODC as a fictive EOD. MS-222 anesthesia silences the EODC output, so the return of EODC output indicates that the fish has recovered from anesthesia (32). At the end of the recording session, the respiration of the fish was switched back to 100 mg/L MS-222 until no EODC output could be recorded, and then the fish was euthanized by freezing.

We obtained intracellular whole cell patch recordings in current clamp, using previously published methods (26, 34, 35). We used glass patch micropipettes with resistances of 20–40 MΩ. The pipette tip was filled with a solution (in mM) of 100 CH_3CO_2K, 2 KCl, 1 $MgCl_2$, 5 EGTA, 10 HEPES, 20 KOH, and 43 biocytin, and the pipette shank was filled with the same solution, except that biocytin was replaced with D-mannitol (26, 34). Initial seal resistances were >1 GΩ. Recordings were amplified 10× and low-pass filtered (cutoff frequency 10 kHz) with an Axopatch 200B amplifier (Molecular Devices), digitized at a rate of 97.7 kHz (model RX8 Digitizer, Tucker Davis Technologies), and saved with custom software written in MATLAB. We delivered electrosensory stimulation using electrodes positioned around the perimeter of the recording chamber (32).

In Vivo Data Collection

After patching a cell, we stimulated with bipolar square pulses, adjusting the duration (0.1–1.5 ms), intensity (3–71 mV/cm), polarity (normal or reversed), and stimulus orientation (transverse or longitudinal to the fish) to elicit maximal subthreshold postsynaptic potential (PSP) amplitudes from each neuron. Next, we injected intracellular depolarizing current, adjusting the duration (1–8 ms) and amplitude (0.1–0.9 nA) until a reliable spike was produced in each neuron. All subsequent sensory and intracellular stimuli delivered during a trial then used these parameters. We did not include in the repetition count any responses to stimulus repetitions in which stimuli occurred within 2–5 ms after an EODC response, since corollary discharge inhibition in the hindbrain blocks sensory responses within this window (23). We only used recordings in which the resting potential varied by 5.5 mV or less across all trials and was at least −40 mV throughout the experiment.

The sensory stimulus was repeated 30 times to get an averaged postsynaptic potential baseline response. The sensory stimulation was then paired with intracellular current injection at the delay of maximum potentiation observed in vitro, −20-ms pre-post delay, or the delay of maximum depression, +10-ms pre-post delay. Three milliseconds was added to each delay time to account for the latency from knollenorgan stimulation to ELa evoked potential for final delays of −23 ms pre-post and +7 ms pre-post. There were three controls: sensory stimulation only, intracellular stimulation only, and no stimulation. All pairings and sensory stimulation-only and intracellular stimulation-only control conditions were repeated at 1 Hz for 6 min. The no-stimulation control lasted 6 min. The order in which they were repeated was decided pseudorandomly, to maintain an equal number of times that each of the two pairings and three controls was collected first. After every pairing or control, sensory stimulation was repeated 30 times to obtain an averaged postsynaptic potential to compare to baseline. To measure the max of the PSP, we found the maximum point in a window from the end of the stimulus to 200 ms. In this same window, to measure the PSP area over time, we summed the poststimulus synaptic potential trace and multiplied by 1 over the sampling frequency (1/sampling frequency = sampling period).

To explore the effect of STDP on EOD tuning, we paired postsynaptic spiking at a potentiating delay of −23 ms pre-post either with a randomly selected conspecific EOD or a 90° phase-shifted version of that same EOD as a sensory stimulus. These EODs were randomly selected from a library of 10 EODs. We adjusted the intensity (3–71 mV/cm) and stimulus orientation (transverse or longitudinal to the fish) to elicit maximal subthreshold PSP amplitudes from each neuron. Both EOD sensory stimuli were repeated 20 times to get an averaged postsynaptic potential baseline response. Which EOD was paired and the order in which they were repeated were decided pseudorandomly, to maintain an

equal number of times that either a natural or a phase-shifted EOD sensory stimulus was collected and to maintain an equal number of natural EOD and phase-shifted EOD pairings. One of the two EOD stimuli, pseudorandomly selected, was paired with intracellular current injection with a −23-ms pre-post delay for 6 min at 1 Hz. Both EOD sensory stimuli were then repeated 20 times to obtain an averaged postsynaptic potential response to compare to baseline. To measure the max of the PSP, we found the maximum point in a window from the end of the stimulus to 200 ms. In this same window, to measure the PSP area over time, we summed the poststimulus synaptic potential trace and multiplied by 1 over the sampling frequency (1/sampling frequency = sampling period).

To explore the effect of STDP on IPI tuning, we paired IPI trains of sensory stimulation with intracellular spiking. We delivered two trains of sensory stimulation: the first train consisted of 10 pulses at 10-ms IPI, and the second train consisted of 10 pulses at 100-ms IPI. Both IPI trains were repeated five times to get an averaged postsynaptic potential baseline response. During pairing, we delivered the 10-ms IPI train, followed by 450 ms of silence, and then the 100-ms IPI train. While this sensory stimulation was delivered, either the 10-ms IPI train or the 100-ms IPI train was paired with 10 pulses of 10-ms IPI or 100-ms IPI postsynaptic spikes with a −23-ms pre-post delay. This pairing was repeated 300 times. The order of the pairings was decided pseudorandomly, to maintain an equal number of times that each condition (pairing with 10-ms IPI or 100-ms IPI) was collected first. After each pairing, IPI sensory stimulation was repeated five times to obtain an averaged postsynaptic potential to compare to baseline. To measure the max of the PSP, we found the maximum point in a window from the end of the first stimulus in the IPI train to the start of the second stimulus in the IPI train. In this same window, to measure the PSP area over time, we summed the poststimulus synaptic potential trace and multiplied by 1 over the sampling frequency (1/sampling frequency = sampling period).

Synaptic Potential Landmarks

In our in vivo experiments, we often observed multiple phases of depolarizations and hyperpolarizations during a postsynaptic potential. We wanted to quantify the physiological characteristics of these synaptic responses to see whether differences in those characteristics correlated with differences in the observed STDP. Synaptic potential landmarks were calculated on the prepairing (i.e., baseline) postsynaptic potential trace for the initial STDP experiments and the EOD tuning experiments and the first baseline postsynaptic potential in the 100-ms IPI train for the IPI tuning experiments. The raw trace was filtered with a 2-ms median filter, and the first and second derivative were both filtered with a 5-ms zero-phase digital filter. Resting potential was calculated by averaging the 50-ms prestimulus period. The baseline postsynaptic potential traces were zeroed by subtracting the resting potential value from the whole trace. The threshold for a depolarization or a hyperpolarization was + or −3 standard deviations from the baseline mean, respectively. We measured 32 different landmarks from each PSP based on 16 different types of measurements. An example of a PSP illustrating these landmarks can be found in Supplemental Fig. S1 (all Supplemental Materials are available at https://doi.org/10.6084/m9.figshare.c.6339569.v2). The landmarks are numbered, and the same numbers are used in Supplemental Fig. S1 and Supplemental Tables S1–S4. These measurements behind these landmarks were defined and measured as follows:

1) Total no. of depolarizations: No. of points that crossed threshold with a positive slope [i.e., *point (i − 1)* < threshold < *point (i)*]
2) Total no. of hyperpolarizations: No. of points that crossed threshold with a negative slope [i.e., *point (i − 1)* > threshold > *point (i)*]
3) Total no. of peaks: No. of local maxima above threshold within a given depolarization; can be >1. The timing of each peak was also recorded. We also set a selection criterion to determine what constitutes a local maximum. We took the first derivative of the trace and recorded all the locations of sign changes in the first derivative trace. To be considered a local maximum, the peak magnitude had to be greater than the maximum value of the poststimulus trace minus the minimum value of the poststimulus trace, divided by 20, from above the first point of a sign change in the first derivative on either side of the peak in question (36).
4) Total no. of troughs: No. of local minima below threshold within a given hyperpolarization; can be >1. The timing of each trough was also recorded. We also set a selection criterion to determine what constitutes a local minimum. We took the first derivative of the trace and recorded all the locations of sign changes in the first derivative trace. To be considered a local minimum, the trough magnitude had to be less than the maximum value of the poststimulus trace minus the minimum value of the poststimulus trace, divided by 20, from below the first point of a sign change in the first derivative on either side of the trough in question (36).
5) Median and range of values of peaks: We measured the median and range (largest peak minus smallest peak) of all the peak amplitudes.
6) Median and range of values of troughs: We measured the median and range (largest trough minus smallest trough) of all the trough amplitudes.
7) Median and range of latencies to all depolarizations and hyperpolarizations: The beginning of a depolarization was defined as the timing of the maximum in the second derivative between the end of the previous depolarization or hyperpolarization and the first peak in the depolarization. If there was no preceding hyperpolarization or depolarization, then the timing of stimulus offset was used instead. The depolarization latency was defined as the beginning of a depolarization minus the time of stimulus offset. The beginning of a hyperpolarization was defined as the timing of the minimum in the second derivative between the end of the previous depolarization or hyperpolarization and the first trough in the hyperpolarization. If there was no preceding hyperpolarization or depolarization, then the time of stimulus offset was used instead. The hyperpolarization latency was defined as the beginning of a hyperpolarization minus the time of stimulus offset. The median and range were

calculated for all the depolarization and hyperpolarization latencies combined.

8) Median and range of latencies to all peaks and troughs: The peak latency was defined as the timing of the peak minus the timing of stimulus offset. The trough latency was defined as the timing of the trough minus the timing of stimulus offset. The median and range were calculated for all the peak and trough latencies combined.

9) Median and range of total duration of each depolarization: Peaks in the second derivative were defined the same as peaks in the PSP (see above), but on the second derivative trace (36). The end of a depolarization was defined as the timing of the first peak in the second derivative after the offset threshold crossing used to define the depolarization. End latency was defined as the end of a depolarization minus the timing of stimulus offset. The total duration of the depolarization was defined as the depolarization end latency minus the depolarization latency. The median and range were calculated for all the depolarization durations.

10) Median and range of total duration of each hyperpolarization: Troughs in the second derivative were defined the same as troughs in the PSP (see above), but on the second derivative trace (36). The end of a hyperpolarization was the time of the first trough in the second derivative after the offset threshold crossing used to define the hyperpolarization. End latency was defined as the end of a hyperpolarization minus the timing of stimulus offset. The total duration of the hyperpolarization was defined as the hyperpolarization end latency minus the hyperpolarization latency. The median and range were calculated for all the hyperpolarization durations.

11) Total PSP duration: Total PSP duration was defined as the end latency of the last depolarization/hyperpolarization minus the first depolarization/hyperpolarization latency.

12) Median and range of duration at half max value of each depolarization: First, we found the value at half of the max, which is the largest peak of a depolarization plus the magnitude at the depolarization latency, divided by 2. Then, we found the timings of half max before and after the largest peak. The duration at half max equaled the timing of half max after peak minus the timing of half max before peak.

13) Median and range of duration at half min value of each hyperpolarization: First, we found the value at half of the min, which is the largest trough of a hyperpolarization plus the magnitude at the hyperpolarization latency, divided by 2. Then, we found the timings of half min before and after the largest trough. The duration at half min equaled the timing of half min after trough minus the timing of half min before trough.

14) Median and range of onset and offset average slope of depolarizations and hyperpolarizations: The depolarization onset slope was calculated by taking the largest peak magnitude of a depolarization minus the depolarization start magnitude, divided by the difference of time between those two points. The hyperpolarization onset slope was calculated by taking the largest trough magnitude of a hyperpolarization minus the hyperpolarization start magnitude, divided by the difference in time between those two points. The depolarization offset slope was calculated by taking the largest peak magnitude of a depolarization minus the depolarization end magnitude, divided by the difference in time between those two points. The hyperpolarization offset slope was calculated by taking the largest trough magnitude of a hyperpolarization minus the hyperpolarization end magnitude, divided by the difference in time between those two points.

15) Summed area of depolarizations and hyperpolarizations: The depolarizations area was calculated by summing all values above threshold and then multiplying by 1 over the sampling frequency (1/sampling frequency = sampling period). The hyperpolarizations area was calculated by summing all values below threshold and then multiplying by 1 over the sampling frequency (1/sampling frequency = sampling period).

16) PSP total area: The total area was calculated by summing the total depolarizations area (described above) and the hyperpolarizations area (described above).

Experimental Design and Statistical Analyses

The goal of this study was to explore the role of STDP in shaping sensory tuning. To do this, we performed experiments in mormyrid weakly electric fish to take advantage of a sensory system in which we could precisely stimulate a sensory system both in vitro and in vivo in a behaviorally relevant way in an intact circuit. The details of the stimulations are stated above for each particular experiment. Unless otherwise stated, values are represented as median and 75%/25% quartiles. The max and area were measured as described above for both baseline PSPs and the PSPs measured after pairing. The area, max, and slope calculations were normalized by subtracting the before-pairing value from the after-pairing value and then dividing by the maximum of the absolute values of the after-pairing and before-pairing values. We used this normalization method because the complex nature of PSPs recorded in vivo made percent change an unreliable measure for two reasons. First, the before-pairing values were sometimes negative, so that an increase would be reflected in a negative percent change and a decrease would be reflected in a positive percent change due to a negative denominator. In addition, the before-pairing values were sometimes very small, so that any change, however small, would be reflected in a very large percent change. Using the maximum of the before- and after-pairing absolute values ensured that the numerator and denominator were of a similar order of magnitude. For the in vitro and in vivo nontuning STDP experiments and pharmacology, a t test was used if there were two groups or one-way ANOVA if there were more than two groups. For the IPI tuning experiments and EOD tuning experiments, a two-way ANOVA was used to compare the stimulus $\times$ pairing interactions. A Bonferroni correction for multiple comparisons was used unless otherwise stated. Details of the synaptic landmark measurements are found in *Synaptic Potential Landmarks*. A principal components analysis (PCA) was performed on the landmarks measured in the in vitro and in vivo experiments. The first four principal components were retained for each. Statistical analysis was done in SPSS and MATLAB.

RESULTS

STDP Alters Synaptic Strength in Midbrain Electrosensory Neurons in Vitro

To test whether we could induce changes in synaptic connectivity via STDP in vitro, we used a whole brain excised preparation from *B. niger* to pair focal ELa presynaptic stimulation with postsynaptic intracellular ELp current injection (Fig. 2*A*) for 6 min at 1 Hz. Because ELa provides topographic, excitatory input to ELp (24) and excitatory ELp-to-ELp connections are more common at shorter distances (27), we expected focal ELa simulation to drive primarily excitatory inputs to the recorded ELp neuron. Presynaptic stimulation was paired with postsynaptic spiking at a range of delays from −80 to +80 ms pre-post. Raw trace examples of synaptic depression evoked by paired stimulation at a 10-ms post-leads-pre delay and synaptic potentiation evoked by a 20-ms pre-leads-post delay are shown in Fig. 2*B*. The PSPs resulting from focal stimulation in vitro consisted primarily of single EPSPs, but examples that deviated from this pattern are shown in Supplemental Fig. S2. We normalized the changes in EPSP amplitude by subtracting the before-pairing values from the after-pairing values and then dividing by the maximum of the absolute values of the after-pairing and before-pairing values. We then plotted the normalized change in EPSP amplitude following paired stimulation against the relative timing of EPSP peaks and postsynaptic action potential peaks during pairing (Fig. 2*C*). There was a clear change in the postsynaptic potential amplitude for delays in the range of −25 to +25 ms between the relative timing of EPSP peaks and postsynaptic action potential peaks (Fig. 2*C*). Using separate exponential curve fits for the pre-leads-post delay data and the post-leads-pre delay data, we found that there was an increase in the synaptic strength as the pre-leads-post delay approached zero and a decrease in the synaptic strength as the post-leads-pre delay approached zero. Correlation coefficients for pre-leads-post delays and post-leads-pre delays were 0.436 and 0.377, respectively.

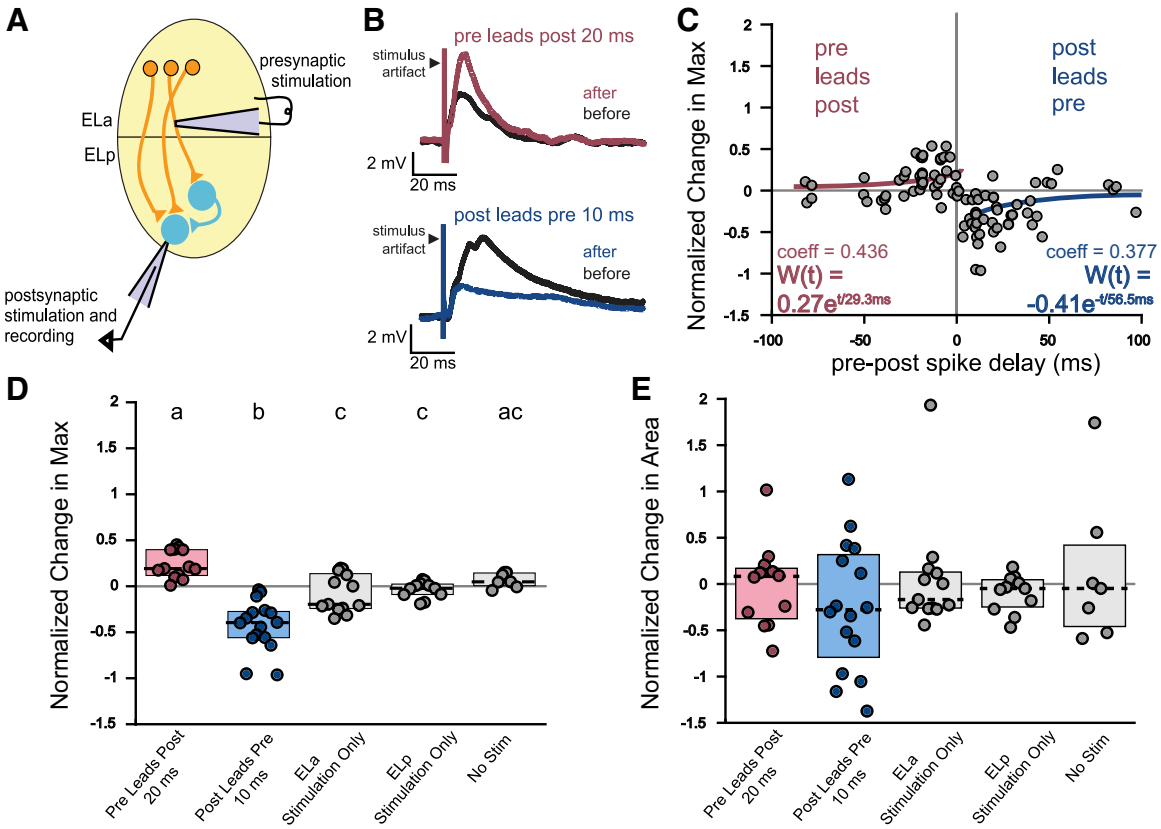

Figure 2. Spike timing-dependent plasticity (STDP) alters synaptic connectivity in vitro. *A*: schematic of the in vitro setup showing focal microstimulation of anterior exterolateral nucleus (ELa) along with intracellular recording and current injection in posterior exterolateral nucleus (ELp). *B*: example raw data traces collected in *Brevimyrus niger* before and after pairing of a −20-ms pre-post delay in red and a +10-ms pre-post delay in blue. *C*: scatterplot of normalized change in excitatory postsynaptic potential (EPSP) amplitude in ELp after pairing ELa stimulation with intracellular current-induced spiking in ELp neurons in *B. niger*. *x*-Axis shows the relative timing of EPSP peaks and postsynaptic action potential peaks. Exponential curve fits with equations and correlation coefficients are provided. *D*: normalized change in EPSP amplitude with median (black dashed line) and quartiles (boxes) for −20-ms pre-post delay in red ($n = 12$), +10-ms pre-post delay in blue (n = 16), and all 3 controls in gray (ELa only $n = 13$, intracellular only $n = 11$, no stimulus $n = 7$). Letters represent statistically significant differences between groups [$P < 0.05$, 1-way ANOVA followed by Tukey's honestly significant difference (HSD) post hoc test]. EPSP amplitudes were normalized by subtracting the before-pairing values from the after-pairing values and then dividing by the maximum of the absolute values of the after-pairing and before-pairing values. *E*: normalized change in EPSP area with median (black dashed line) and quartiles (boxes) for −20-ms pre-post delay in red ($n = 12$), +10-ms pre-post delay in blue ($n = 16$), and all 3 controls in gray (ELa only $n = 13$, intracellular only $n = 11$, no stimulus $n = 7$). EPSP areas were normalized by subtracting the before-pairing values from the after-pairing values and then dividing by the maximum of the absolute values of the after-pairing and before-pairing values.

After averaging all the changes at each pre-post stimulus delay, we found that the stimulus delays of −20 ms pre-post and +10 ms pre-post evoked the largest potentiation and depression, respectively. We also included three different controls, in addition to these two pairings: presynaptic ELa stimulation only, postsynaptic ELp spiking only, and no stimulus. ELa stimulation-only and postsynaptic ELp spiking-only controls were also performed for 6 min at 1 Hz, and the no-stimulus control period lasted for 6 min. Since STDP depends on the correlation between pre- and postsynaptic spiking, we chose these controls to elucidate any plasticity or changes in excitability that may be due to factors other than STDP. We found a significant difference in EPSP amplitude changes after paired stimulation among the −20 ms pre-post pairing, the +10 ms pre-post pairing, and controls [Fig. 2*D*; $F(4,54) = 21.893$, $P < 0.0005$, 1-way ANOVA]. Specifically, we found that the −20 ms pre-post synaptic pairing was significantly different from the +10 ms pre-post synaptic pairing [$P < 0.0005$, Tukey's honestly significant difference (HSD)]. The −20 ms pre-post synaptic pairing was also significantly different from the ELa stimulation-only control ($P = 0.002$, Tukey's HSD) and the intracellular spiking-only control ($P < 0.014$, Tukey's HSD), but there was no significant difference between the −20 ms pre-post synaptic pairing and the no-stimulus control ($P = 0.401$, Tukey's HSD). The +10 ms pre-post pairing was significantly different from the ELa stimulation-only control ($P < 0.0005$, Tukey's HSD), the intracellular spiking-only control ($P < 0.0005$, Tukey's HSD), and the no-stimulus control ($P < 0.0005$, Tukey's HSD). The ELa-only control was not significantly different from the intracellular-only control ($P = 0.981$, Tukey's HSD) or the no-stimulus control ($P = 0.483$, Tukey's HSD), nor was the intracellular-only control significantly different from the no-stimulus control ($P = 0.797$, Tukey's HSD) (Fig. 2*D*).

We normalized the changes in EPSP area by subtracting the before-pairing values from the after-pairing values and then dividing by the maximum of the absolute values of the after-pairing and before-pairing values. We found no significant difference in the normalized change in EPSP area after paired stimulation between the −20 ms pre-post and +10 ms pre-post pairings and controls [Fig. 2*E*; $F(4,54) = 0.724$, $P = 0.579$, 1-way ANOVA].

To determine whether STDP is broadly consistent across species, we paired pre- and postsynaptic stimulation in *B. brachyistius* at both −20-ms pre-post and +10-ms pre-post delays. When comparing normalized change in max, the former resulted in potentiation whereas the latter resulted in depression [$t(27) = 3.291$, $P = 0.0027$, paired *t* test; Supplemental Fig. S3A). We found no significant difference in the normalized change in area [$t(27) = 1.645$, $P = 0.1112$, paired *t* test; Supplemental Fig. S3B), though visually there is a trending difference. The results suggest that synaptic connectivity in ELp can be altered by STDP in both species studied. To induce STDP in all experiments that follow, we used −20-ms pre-post stimulus delays to induce potentiation and +10-ms pre-post stimulus delays to induce depression.

Induction of STDP Requires NMDA Receptors

ELp neurons are known to have both NMDA and AMPA receptors (27), and NMDA receptors are a known mediator of long-term potentiation (LTP) (11). Therefore, we tested the role of NMDA and AMPA receptors in STDP by bath perfusion of either APV, an antagonist of NMDA receptors, or DNQX, an antagonist of AMPA receptors, in *B. niger*. There were significant differences in the baseline EPSP amplitudes between control, DNQX application, and APV application [Fig. 3*A*; $F(2,57) = 10.631$, $P < 0.0005$, 1-way ANOVA]. DNQX application resulted in a significant decrease in EPSP amplitude compared with control ($P < 0.0005$, Tukey's HSD), whereas APV application did not cause a significant decrease in EPSP amplitude compared with control ($P = 0.475$, Tukey's HSD) (Fig. 3*A*). As a result, EPSP amplitudes in the presence of DNQX were significantly smaller than EPSP amplitudes in the presence of APV ($P = 0.014$, Tukey's HSD).

Both APV and DNQX application resulted in a significant decrease in potentiation elicited by the −20-ms pre-post

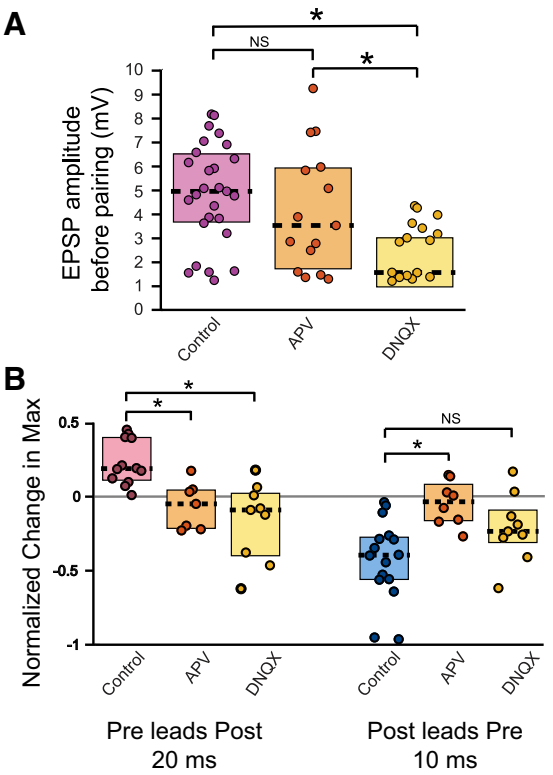

Figure 3. Spike timing-dependent plasticity (STDP) is NMDA receptor dependent. *A*: excitatory postsynaptic potential (EPSP) amplitude of baseline responses before pairing for control data (purple, $n = 27$), during DL-2-amino-5-phosphonopentanoic acid (APV) application (orange, $n = 15$), and during 6,7-dinitroquinoxaline-2,3-dione (DNQX) application (yellow, $n = 18$), all collected in *Brevimyrus niger*. Median values are shown with black dashed lines, and quartiles are represented by boxes. *Statistically significant differences between groups ($P < 0.05$, unpaired *t* test). NS, not significant. *B*: normalized change in EPSP amplitude after pairing anterior exterolateral nucleus (ELa) stimulation with intracellular current-induced spiking in posterior exterolateral nucleus (ELp) neurons at a −20-ms pre-post delay (*left*) and a +10-ms pre-post delay (*right*), showing the median (black dashed line) and quartiles (boxes) under control conditions (red, $n = 12$; blue, $n = 16$), during APV application (orange, $n = 7$ and $n = 8$), and during DNQX application (yellow, $n = 9$ and $n = 9$), all collected in *B. niger*. *Statistically significant differences between groups ($P < 0.05$, unpaired *t* test). EPSP amplitudes were normalized by subtracting the before-pairing values from the after-pairing values and then dividing by the maximum of the absolute values of the after-pairing and before-pairing values.

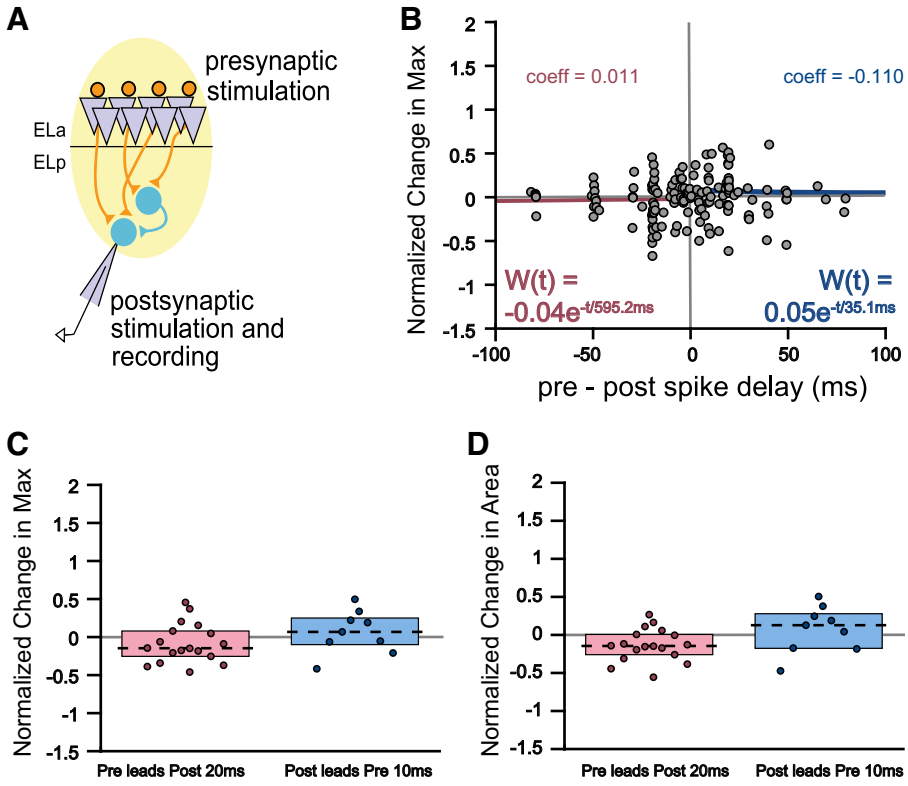

Figure 4. Stimulating anterior exterolateral nucleus (ELa) with an array electrode reveals more variation in spike timing-dependent plasticity (STDP) compared with focal stimulation in vitro. *A*: a schematic of the in vitro array setup showing 4-channel stimulation of ELa along with intracellular current injection in posterior exterolateral nucleus (ELp). *B*: scatterplot of normalized change in excitatory postsynaptic potential (EPSP) amplitude in ELp after ELa array stimulation; data collected in *Brevimyrus niger*. *x*-Axis shows the relative timing of EPSP peaks and postsynaptic action potential peaks. (n = 128). EPSP amplitudes were normalized by subtracting the before-pairing values from the after-pairing values and then dividing by the maximum of the absolute values of the after-pairing and before-pairing values. Exponential curve fits with equations and correlation coefficients are provided. *C*: normalized change in EPSP max after pairing ELa array stimulation with intracellular current-induced spiking in ELp neurons at a −20-ms pre-post delay (*left*) and a +10-ms pre-post delay (*right*), showing the median (black dashed line) and quartiles (boxes) under control conditions (red, n = 18; blue, n = 9). EPSP amplitudes were normalized by subtracting the before-pairing values from the after-pairing values and then dividing by the maximum of the absolute values of the after-pairing and before-pairing values. *D*: normalized change in EPSP area after pairing ELa array stimulation with intracellular current-induced spiking in ELp neurons at a −20-ms pre-post delay (*left*) and a +10-ms pre-post delay (*right*), showing the median (black dashed line) and quartiles (boxes) under control conditions (red, n = 18; blue, n = 9). EPSP areas were normalized by subtracting the before-pairing values from the after-pairing values and then dividing by the maximum of the absolute values of the after-pairing and before-pairing values.

delay [Fig. 3*B*; $t(17) = 3.98$, $P = 0.00095$, unpaired t test; −20-ms pre-post delay vs. DNQX −20-ms pre-post, $t(19) = 5.31$, $P = 0.00004$, unpaired t test]. APV but not DNQX application resulted in a significant decrease in depression elicited by a +10-ms pre-post delay [Fig. 3*B*; $t(22) = -3.67$, $P = 0.0013$, unpaired t test; +10-ms pre-post delay vs. DNQX +10-ms pre-post, $t(23) = -1.98$, $P = 0.059$, unpaired t test]. Since blocking NMDA receptors did not have a significant effect on EPSP amplitudes, these results suggest that NMDA receptors are necessary for the synaptic strength changes elicited by STDP. The effect of DNQX on STDP likely reflects the significant reduction in EPSP amplitudes caused by blocking AMPA receptors, as a reduction in EPSP amplitude is expected to reduce the magnitude of synaptic plasticity.

Diffuse Presynaptic Stimulation Induces Variable STDP

A given EOD stimulates a distinct subpopulation of cells in the ELa (21, 25), and the ELa provides topographic, excitatory input to the ELp (24). An array of stimulus electrodes stimulates both focal ELa inputs that provide direct excitatory input to the recorded neuron and adjacent ELp neurons as well as excitatory input to more distant ELp neurons (22). Because excitatory ELp-to-ELp connections tend to occur over short distances (27), array stimulation in vitro is expected to stimulate more inhibitory inputs to recorded neurons compared with pathways excited by focal ELa stimulation. In *B. niger*, when postsynaptic ELp spikes were paired with presynaptic stimulation using a large electrode array in ELa (Fig. 4*A*), the resulting changes in EPSP amplitude were more variable (Fig. 4*B*). No large changes in EPSP amplitude were observed for relatively long pre-leads-postsynaptic delays or long post-leads-presynaptic delays. However, at relatively short pre-leads-post delays both potentiation and depression were observed, and a similar pattern was observed at relatively short post-leads-pre delays (Fig. 4*B*). Using separate exponential curve fits for the pre-leads-post delay data and the post-leads-pre delay data, we found that the fit for both delays did not match the pattern observed with focal in vitro stimulation. Correlation coefficients for pre-leads-post delays and post-leads-pre delays were 0.011 and −0.110, respectively (Fig. 4*B*). These results show that stimulating a larger, more diffuse population of ELa neurons can result in a more variable pattern of STDP at both positive and negative pre-post delays close to zero, compared with focal ELa stimulation. Comparing the normalized change in max measurement, we found that the −20 ms pre-post synaptic pairing was not significantly different from the +10 ms pre-post synaptic pairing [Fig. 4*C*; $t(25) = -1.36$, $P = 0.187$, unpaired t test]. Comparing the normalized change in area measurement, we similarly found that the −20 ms pre-post synaptic pairing was not significantly different from the +10 ms pre-post synaptic pairing [Fig. 4*D*; $t(25) = -2.05$, $P = 0.051$, unpaired t test].

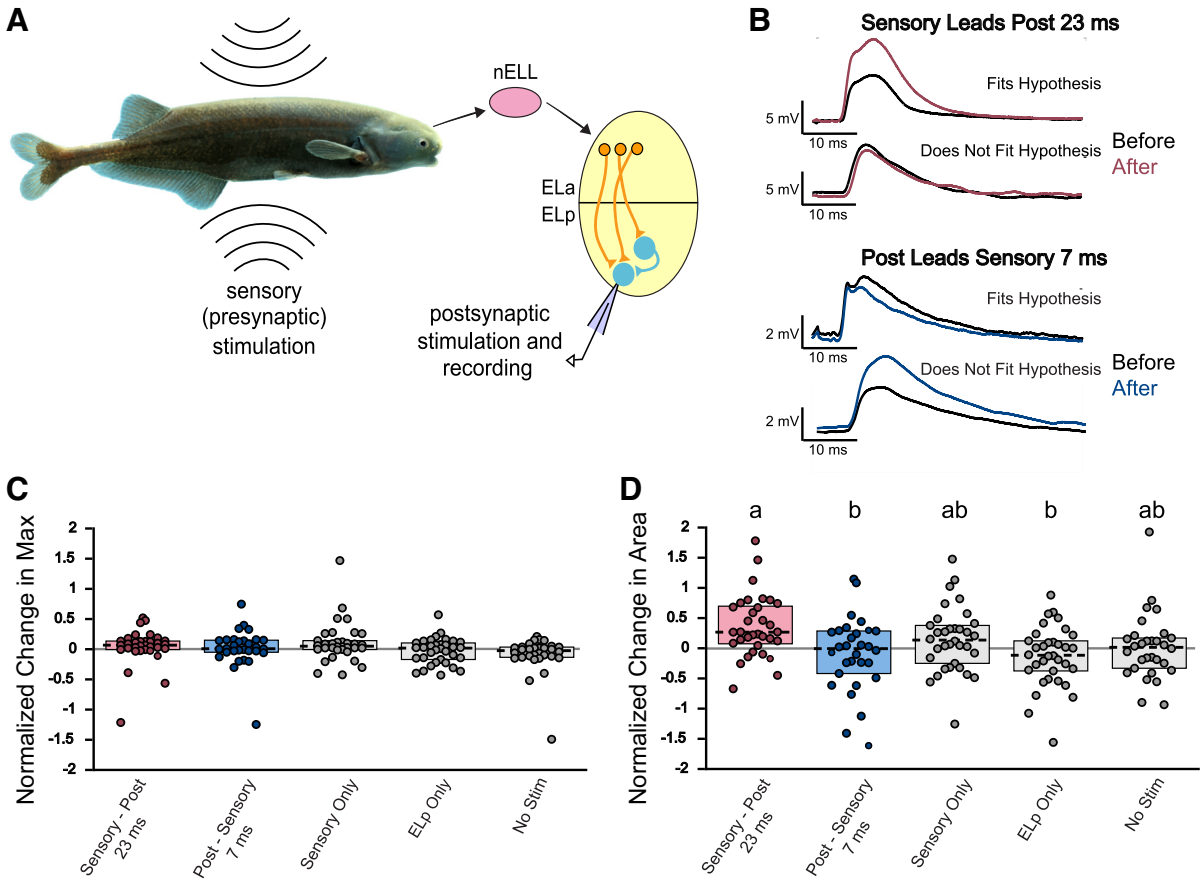

Figure 5. Spike timing-dependent plasticity (STDP) alters synaptic connectivity in vivo. *A*: a model of the in vivo setup showing sensory stimulation along with intracellular current injection in posterior exterolateral nucleus (ELp). ELa, anterior exterolateral nucleus; nELL, nucleus of the electrosensory lateral line lobe. *B*: example raw data traces collected in *Brevimyrus niger* before and after pairing of a −23-ms sensory-post delay in red and a +7-ms sensory-post delay in blue. One example each of changes that fit the STDP pattern observed in vitro and that do not fit the STDP pattern observed in vitro are shown. *C*: normalized change in max (after-before) values with median (black dashed line) and quartiles (boxes) for −20-ms sensory-post delay in red (n = 33), 10-ms sensory-post delay in blue (n = 30), and all 3 controls in gray (sensory only n = 34, intracellular only n = 34, no stimulus n = 30). Excitatory postsynaptic potential (EPSP) amplitudes were normalized by subtracting the before-pairing values from the after-pairing values and then dividing by the maximum of the absolute values of the after-pairing and before-pairing values. *D*: same as in *C* but showing normalized change in area values rather than normalized change in max values. Letters represent statistically significant differences between groups ($P < 0.05$, 1-way ANOVA followed by Tukey's HSD post hoc test). EPSP areas were normalized by subtracting the before-pairing values from the after-pairing values and then dividing by the absolute value of the maximum of the after-pairing and before-pairing values.

STDP Can Alter Synaptic Connectivity in Vivo

Next, we sought to determine whether STDP could be induced in vivo in response to pairing sensory stimuli with postsynaptic spiking. In these experiments in *B. niger*, we provided presynaptic input using sensory stimulation rather than direct stimulation of ELa while recording intracellularly from ELp neurons (Fig. 5*A*). We paired sensory stimulation with intracellular stimulation, using delays that generally resulted in strong potentiation (−20 ms pre-post) versus depression (+10 ms pre-post) in vitro (see Fig. 2*D*). However, for both pairings we added a 3-ms delay to account for the latency between sensory stimulation and ELa responses (37). Thus, we delivered paired stimulation with sensory stimulation leading postsynaptic stimulation by 23 ms and sensory stimulation following postsynaptic stimulation by 7 ms, as well as three controls: sensory stimulation only, intracellular stimulation only, and no stimulation.

Although many of the changes in synaptic responses fit the predicted patterns of potentiation in response to the sensory-leads-post pairing and depression in response to the post-leads-sensory pairing, many others did not (Fig. 5*B*). Unlike the focal in vitro data, no significant differences were found among the five treatments for normalized change in PSP maximum values (Fig. 5*C*; P = 0.089, 1-way ANOVA). However, there were significant differences among the treatments for normalized change in area (Fig. 5*D*; P = 0.002, 1-way ANOVA). In particular, the sensory-leads-post pairing was significantly larger than the post-leads-sensory pairing (Fig. 5*D*; P = 0.009, Tukey's HSD). Results of the other pairwise comparisons are as follows: sensory-leads-post vs. sensory stimulus only, P = 0.466; sensory-leads-post vs. intracellular only, P = 0.002; sensory-leads-post vs. no stimulus, P = 0.088; post-leads-sensory vs. sensory stimulus only, P = 0.404; post-leads-sensory vs. intracellular only, P = 0.998; post-leads-sensory vs. no stimulus, P = 0.934; sensory only vs. intracellular only, P = 0.222; sensory only vs.

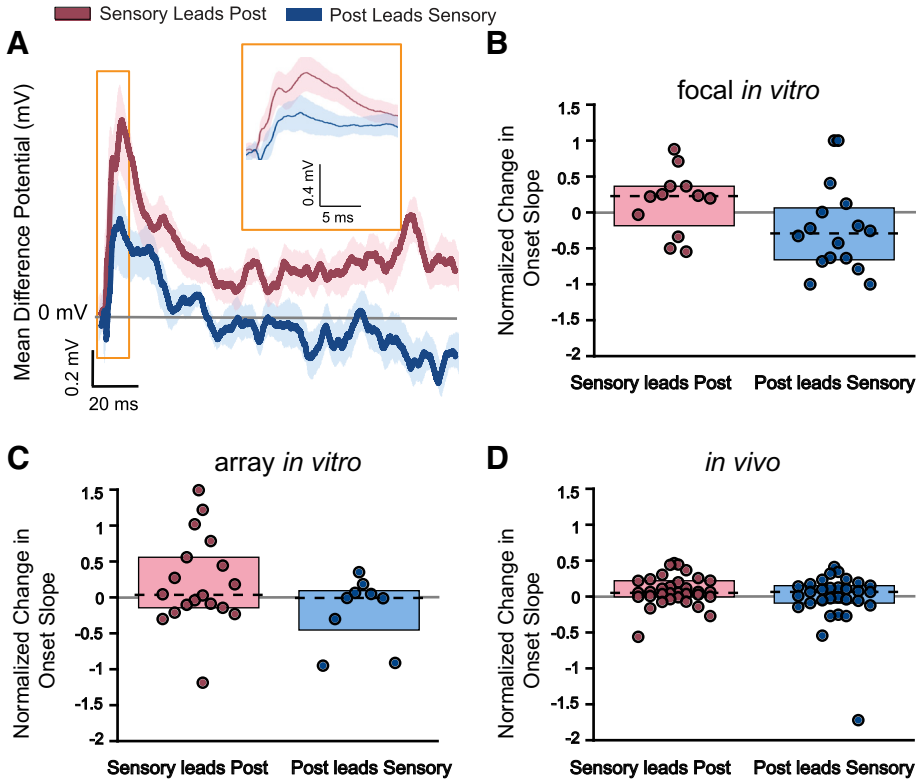

Figure 6. Spike timing-dependent plasticity (STDP) affects synaptic activity later than 7 ms after stimulus onset. *A*: average after pairing – before pairing traces collected in *Brevimyrus niger* for −23-ms sensory-post delay (red) and +7-ms sensory-post delay (blue). *Time = 0* at stimulus onset. Gray line is 0 mV. Lighter-colored areas surrounding the traces represent SE. *Inset*, zoomed-in view of the area surrounding the peaks of the traces. *B–D*: normalized change in onset slope for focal in vitro data [*B*; −20-ms pre-post delay in red (n = 12), 10-ms pre-post delay in blue (n = 16)], array in vitro data [*C*; −20-ms pre-post delay in red (n = 18), 10-ms pre-post delay in blue (n = 9)], and in vivo data [*D*; −23-ms sensory-post delay in red (n = 33), 7-ms sensory-post delay in blue (n = 30)]. Excitatory postsynaptic potential (EPSP) slopes were normalized by subtracting the before-pairing values from the after-pairing values and then dividing by the maximum of the absolute values of the after-pairing and before-pairing values.

no stimulus, P = 0.880; intracellular only vs. no stimulus, P = 0.807 (all pairwise comparisons using Tukey's HSD).

To analyze the time course of these changes in synaptic responses, we subtracted the mean voltage trace before pairing from the mean voltage trace after pairing and then averaged across neurons to obtain a mean difference potential that represents the overall time course of changes in synaptic response. The maximum change in synaptic response occurred at 14.5 ms after stimulus onset for sensory-leads-post and 13.4 ms for post-leads-sensory (Fig. 6*A*). Although there is a positive peak in the post-leads-sensory trace, the positive peak in the sensory-leads-post trace is larger, which shows that there is a relative increase in synaptic strength in the sensory-leads-post delay relative to the post-leads-sensory delay. In addition, because of the later shape of the post-leads-sensory delay PSP, which reveals a decrease in synaptic strength, the overall change in area is closer to zero for the post-leads-sensory trace. We also analyzed the normalized change in onset slope for the focal in vitro data, the array in vitro data, and the in vivo data and found no significant differences [Fig. 6*B*: $t(26)$ = 1.79, P = 0.084, unpaired t test; Fig. 6*C*: $t(25)$ = 1.58, P = 0.126, unpaired t test; Fig. 6*D*: $t(61)$ = 1.36, P = 0.178, unpaired t test].

The Induction of STDP Varies with the Physiological Characteristics of Synaptic Responses

Whereas the postsynaptic potentials recorded in vitro typically consisted almost exclusively of excitatory postsynaptic potentials with a single peak, the postsynaptic potentials recorded in vivo often contained both positive and negative components consisting of multiple peaks and troughs (Fig. 7*A*). To determine whether there are physiological attributes of neurons that might relate to the widespread variation we observed in STDP during in vitro array stimulation and in vivo sensory stimulation (see Fig. 4*B* and Fig. 5, *B–D*), we measured 16 landmarks from the postsynaptic potentials of each neuron before pairing (see MATERIALS AND METHODS and Supplemental Materials for details). We performed a principal components analysis (PCA) on these landmarks and then ran a two-way ANOVA on the resulting PC scores in which the independent variables included pairing (pre-leads-post vs. post-leads-pre) and whether or not the observed change in postsynaptic potential after pairing fit our STDP predictions based on the normalized change in max data (i.e., a positive change in normalized max for a pre-leads-post delay and a negative change in normalized max for a post-leads-pre delay would fit our hypothesis). The specific eigenvalue loadings and the landmarks they represent can be found in the Supplemental Materials.

For the in vitro focal stimulation data, when reviewing the normalized change in max amplitude, there were no values that did not fit the expected STDP direction. For the in vitro array stimulation data (Fig. 7*B*), there were N = 12 pre-leads-post pairings that fit the hypothesis and N = 6 that did not fit. There were N = 4 post-leads-pre pairings that fit the hypothesis and N = 5 that did not fit. The first four PC scores captured 76.67% of the variance. We found significant differences for PC 3. For PC3, the "fit" variable was significantly different [$F(1,18)$ = 7.05, P = 0.016, 2-way ANOVA] and the "pairing" variable was significantly different [$F(1,18)$ = 8.81, P = 0.008, 2-way ANOVA]. In the eigenvalue loadings found in Supplemental Table S1, for PC3 negative loadings are dominated by landmarks relating to hyperpolarizations,

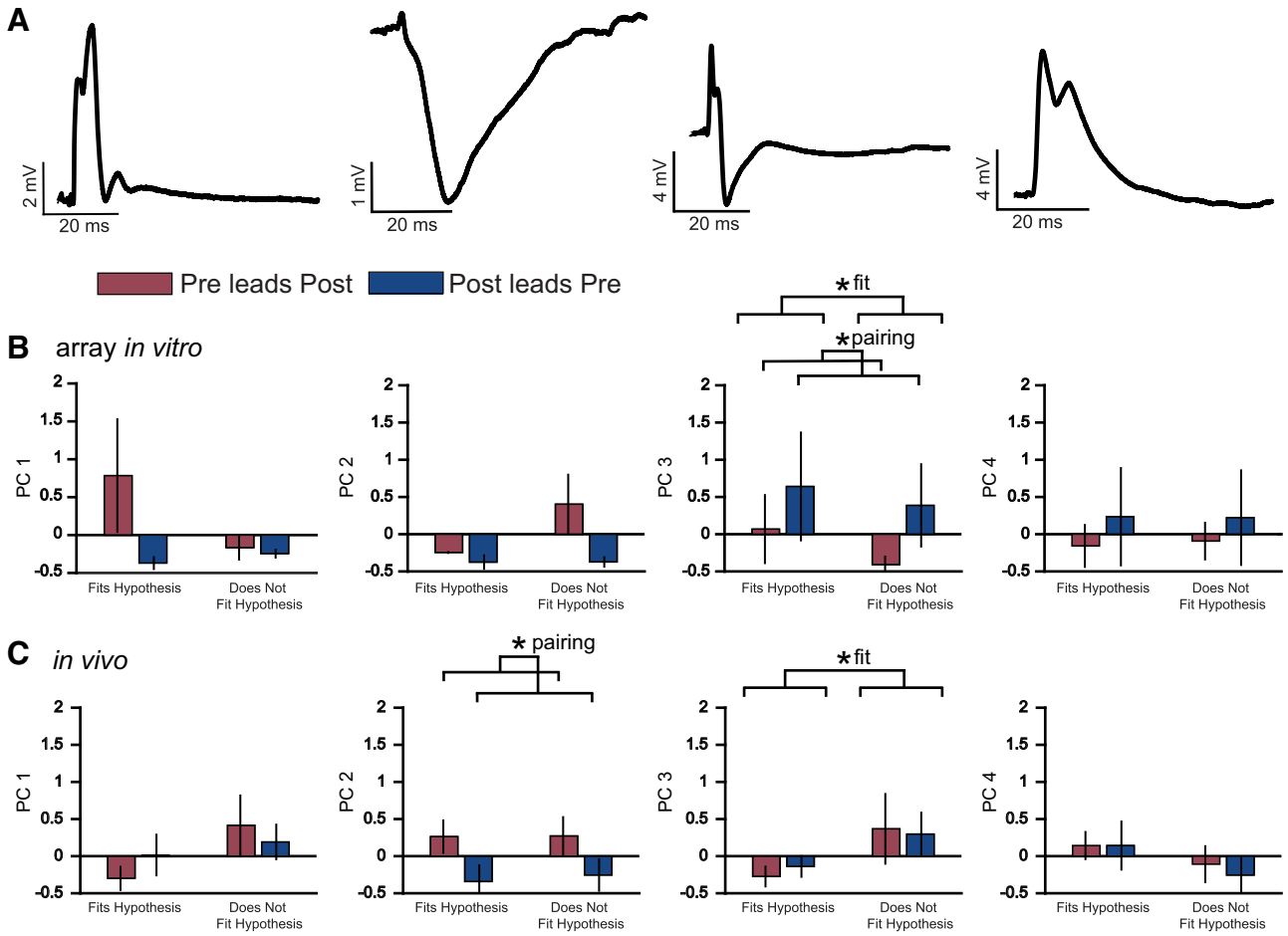

Figure 7. Variation in the effect of spike timing-dependent plasticity (STDP) is correlated with variation in synaptic responses. *A*: raw trace examples of postsynaptic potentials recorded in vivo in *Brevimyrus niger*. *B*: principal components (PCs) 1–4 for the in vitro array data that "fit" or "do not fit" the STDP hypothesis based on the in vitro data for both −20-ms pre-post delay (red) and +10-ms pre-post delay (blue). *Significantly different variable or interaction stated in the text. *C*: PCs 1–4 for the in vivo data that "fit" or "do not fit" the STDP hypothesis based on the in vitro data for both −23-ms sensory-post delay (red) and +7-ms sensory-post delay (blue). *Significantly different variable or interaction stated in the text.

whereas positive loadings are dominated by landmarks relating to depolarizations. This suggests that the relative balance of excitatory and inhibitory pathways leading to the recorded neuron is affecting whether the array in vitro data fit the STDP direction predicted by the focal in vitro data. For the in vivo data (Fig. 7*C*), there were $N = 24$ sensory-leads-post pairings that fit the hypothesis and $N = 9$ that did not fit. There were $N = 13$ post-leads-sensory pairings that fit the hypothesis and $N = 17$ that did not fit. The first four PC scores captured 76.31% of the variance. We found significant differences in PCs 2 and 3. For PC2 data the "pairing" variable was significant [$F(1,59) = 4.598$, $P = 0.036$, 2-way ANOVA]. For PC3, the "fit" variable was significantly different [$F(1,59) = 4.162$, $P = 0.046$, 2-way ANOVA]. Although the loadings did not separate into easily discernable categories (Supplemental Table S2), there were still significant differences in the PCs, which suggests that differences in the excitatory- and inhibitory-based synaptic landmarks relate to whether the in vivo data did or did not fit the expected STDP direction based on the focal in vitro data. Together, these results suggest that physiological characteristics of postsynaptic potential responses relate to whether the induction of STDP results in synaptic connectivity changes in the direction predicted by the in vitro focal stimulation results.

STDP Does Not Cause Changes to Different EOD Stimuli as Predicted by in Vitro Focal Stimulation Data

We next sought to determine whether STDP could elicit selective changes in the synaptic responses to particular EOD stimuli. In this experiment in *B. brachyistius*, we presented a randomly chosen conspecific EOD and a 90° phase-shifted version of that EOD as sensory stimuli. The latter manipulation maximally distorts the EOD waveform in the temporal domain while keeping the frequency spectrum constant (28, 38). After recording responses to both stimuli, we randomly selected one of the two stimuli to pair with intracellular stimulation at a −23-ms sensory-leads-post delay. We then recorded responses to both stimuli after pairing to determine whether there was a selective increase in synaptic response to the paired stimulus. We found no significant differences for either the normalized change in area or the normalized change in max data (Fig. 8). However, some experiments did result in selective increases in response to the paired stimulus, as shown by the gray lines connecting data points from the same neurons.

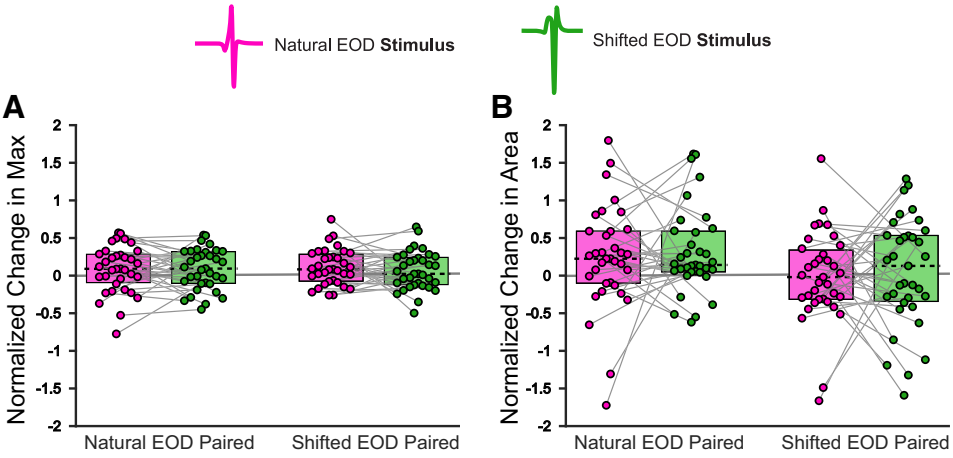

Figure 8. Spike timing-dependent plasticity (STDP) does not cause changes to different electric organ discharge (EOD) stimuli as predicted by in vitro focal stimulation data. *A*: normalized change in max values with median (black dashed line) and quartiles (boxes) for natural EODs (magenta, n = 35) and phase-shifted EODs (green, n = 25). Gray lines connect data points collected during the same trial from the same neuron. Data collected in *Brienomyrus brachyistius*. Excitatory postsynaptic potential (EPSP) amplitudes were normalized by subtracting the before-pairing values from the after-pairing values and then dividing by the maximum of the absolute values of the after-pairing and before-pairing values. *B*: same as in *A* but with normalized change in area values rather than normalized change in max values. EPSP areas were normalized by subtracting the before-pairing values from the after-pairing values and then dividing by the maximum of the absolute values of the after-pairing and before-pairing values.

STDP Can Cause Selective Changes in the Responses to Different IPI Stimuli

Within this sensory pathway, ELa neurons respond faithfully to a given EOD stimulus regardless of IPI, and IPI tuning first arises within ELp (26). Thus, we were able to test whether STDP could elicit selective changes in the responses to different IPI stimuli both in vitro and in vivo. In both cases, in *B. niger*, we repeatedly delivered trains of 10-ms and 100-ms IPIs while pairing postsynaptic stimulation with just one of the IPIs at a pre-leads-post delay of −20 ms (or sensory-leads-post delay of −23 ms) (Fig. 9*A*). We then measured the change in response to both 10-ms and 100-ms IPIs after pairing. In vitro, we found clear evidence for a differential shift in responses to 10- versus 100-ms IPIs depending on which IPI postsynaptic spikes were paired with, resulting in a significant "stimulus" × "pairing" interaction effect for the normalized change in max value (Fig. 9*B*; $F(1,26)$ = 7.42, P = 0.011, 2-way repeated-measures ANOVA]. Pairing with 10-ms IPIs led to a relative increase in synaptic responses to 10-ms IPIs compared with 100-ms IPIs, whereas pairing with 100-ms IPIs led to a relative increase in synaptic responses to 100-ms IPIs compared with 10-ms IPIs (Fig. 9*B*). There was no significant interaction effect in the normalized change in area measurement, though there was a qualitative increase in the 100-ms IPI stimulus relative to the 10-ms IPI stimulus after pairing with a 100-ms IPI (Fig. 9*C*). In vivo, however, there were no significant differences for changes in either the normalized max or area for the 10-ms or 100-ms IPI pairings (Fig. 9, *D* and *E*).

In Vivo EOD and IPI Tuning Varies with the Physiological Characteristics of Synaptic Responses

Some EOD and IPI sensory tuning experiments did result in selective increases in response to the paired stimulus, as shown by the gray lines connecting data points from the same neurons in Fig. 8 and Fig. 9. Therefore, we performed a landmark calculation and PCA analysis on these data to determine whether physiological characteristics of synaptic responses could predict the shift in responses to paired and unpaired EOD and IPI stimuli. For the in vivo EOD tuning experiments, there were N = 38 natural EOD pairings that fit the hypothesis and N = 32 that did not fit. There were N = 36 shifted EOD pairings that fit the hypothesis and N = 34 that did not fit. The first four PC scores captured 58.9% of the variance. PC1 and PC4 had significant "fit" × "pairing" interactions [Fig. 10*A*; $F(1,136)$ = 7.03, P = 0.009, 2-way ANOVA and $F(1,136)$ = 6.59, P = 0.011, 2-way ANOVA]. In the eigenvalue loadings found in Supplemental Table S3, for PC1 negative loadings are dominated by landmarks relating to depolarizations whereas positive loadings are dominated by landmarks relating to hyperpolarizations. This suggests that the relative balance of excitatory and inhibitory pathways leading to the recorded neuron is affecting whether the EOD tuning data fit the STDP direction predicted by the focal in vitro data. For PC4, although the loadings did not separate into easily discernable categories, there were still significant differences in the PC, which suggests that differences in the excitatory- and inhibitory-based synaptic landmarks relate to whether the EOD tuning data did or did not fit the expected STDP direction based on the focal in vitro data. For the in vivo IPI tuning experiments, there were N = 7 10-ms pairings that fit the hypothesis and N = 11 that did not fit. There were N = 7 100-ms pairings that fit the hypothesis and N = 10 that did not fit. The first four PC scores captured 71% of the variance. There were no significant differences in the PCs based on IPI, though there are qualitative differences in the graphs (Fig. 10*B*, Supplemental Table S4). These results suggest that physiological characteristics of postsynaptic potential responses relate to whether EOD and IPI tuning results in synaptic connectivity changes in the direction predicted by the in vitro focal stimulation results.

DISCUSSION

In vitro studies across many brain regions and organisms have shown that repeated pre-leads-postsynaptic spiking induces synaptic potentiation, whereas the reverse timing induces synaptic depression (12, 13, 39). This Hebbian form

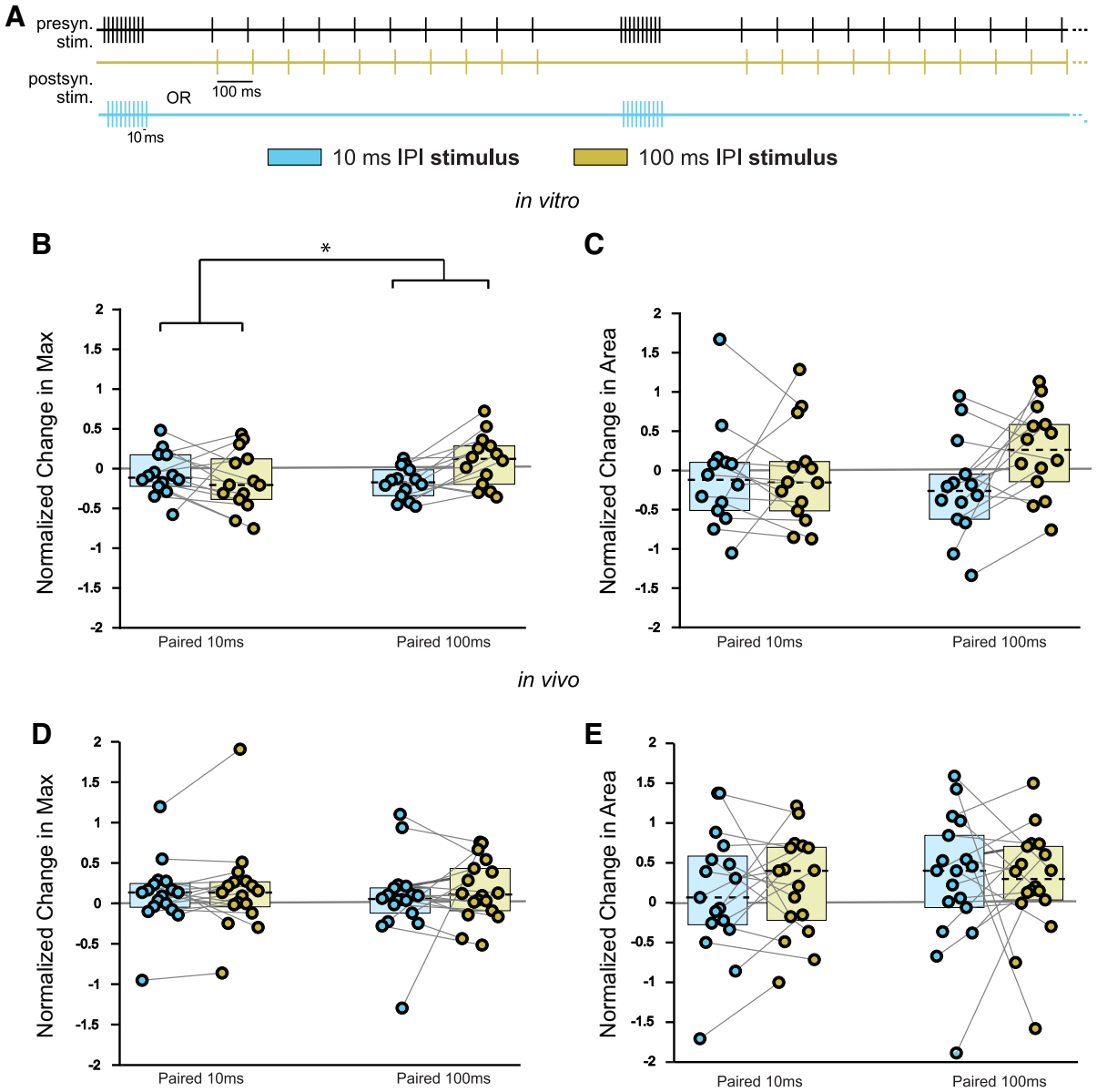

Figure 9. Spike timing-dependent plasticity (STDP) alters interpulse interval (IPI) tuning in vitro but does not cause similar changes to different IPI stimuli in vivo as predicted by in vitro focal stimulation. *A*: model of the stimulation protocol, showing an alternating train of 10-ms and 100-ms IPIs in black with intracellular current injection in the posterior exterolateral nucleus (ELp) only paired with either the 10-ms IPI (blue, $n = 14$) or 100-ms IPI (yellow, $n = 14$). *B*: in vitro normalized change in max amplitude values with median (black dashed line) and quartiles (boxes) for the paired IPI compared with the unpaired IPI ($N = 14$ for all pairings). Data collected in *Brevimyrus niger*. *Statistically significant interaction effect between "stimulus" × "pairing" variables ($P < 0.05$, 2-way ANOVA). Excitatory postsynaptic potential (EPSP) amplitudes were normalized by subtracting the before-pairing values from the after-pairing values and then dividing by the maximum of the absolute values of the after-pairing and before-pairing values. *C*: same as *B* but with normalized change in area values instead of normalized change in max values. EPSP areas were normalized by subtracting the before-pairing values from the after-pairing values and then dividing by the maximum of the absolute values of the after-pairing and before-pairing values. *D*: normalized change in max values with median (black dashed line) and quartiles (boxes) comparing the paired IPI (paired 10 ms $n = 18$; paired 100 ms $n = 17$) to the unpaired IPI. Data collected in *B. niger*. Gray lines are connecting data points collected during the same trial in the same neuron. EPSP amplitudes were normalized by subtracting the before-pairing values from the after-pairing values and then dividing by the maximum of the absolute values of the after-pairing and before-pairing values. *E*: same as *D* but with normalized change in area values instead of normalized change in max values. EPSP areas were normalized by subtracting the before-pairing values from the after-pairing values and then dividing by the maximum of the absolute values of the after-pairing and before-pairing values.

of STDP has been implemented in a variety of computational models that explore many circuits (40–42). Additionally, it is known that STDP can alter neuronal responses to sensory input in vivo (11), and we describe a few examples below in more detail. However, these studies in adult organisms are specific to the role of STDP in processing self-generated sensory representations or reinforcing stable sensory representations, rather than how STDP alters sensory tuning to stimuli in a changing sensory environment. The role of STDP in altering tuning to external stimuli in intact adult

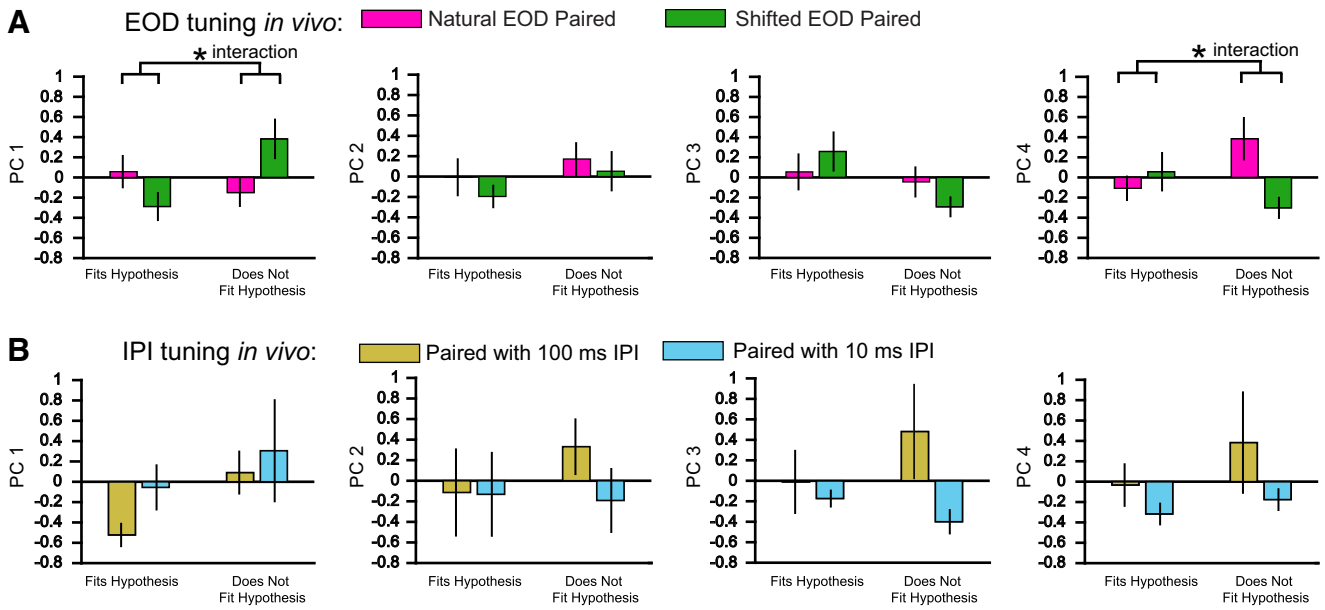

Figure 10. Variation in the effect of spike timing-dependent plasticity (STDP) on tuning is correlated with variation in synaptic responses. *A*: principal components (PCs) 1–4 for the in vivo electric organ discharge (EOD) tuning data that "fit" or "do not fit" the STDP hypothesis for natural EOD pairing (magenta) and shifted EOD pairing (green). *Significantly different variable or interaction stated in the text. *B*: PCs 1–4 for the in vivo interpulse interval (IPI) data that "fit" or "do not fit" the STDP hypothesis for both 10 ms pairing (blue) and 100 ms pairing (yellow).

circuits in real time remains unclear. We leveraged studying sensory processing in mormyrid weakly electric fish, a system where we have precise control over the timing of presynaptic input using behaviorally relevant stimuli both in vitro and in vivo. We show for the first time in ELp neurons that there is clear synaptic potentiation at pre-leads- postsynaptic delays and clear synaptic depression at post-leads-presynaptic delays in vitro with focal stimulation (Fig. 2), indicative of Hebbian STDP.

Once we established that Hebbian STDP can be induced in ELp neurons, we explored the role of STDP in altering sensory tuning. In vitro, pairing with 10-ms IPIs led to a relative increase in synaptic responses to 10-ms IPIs compared with 100-ms IPIs, whereas pairing with 100-ms IPIs led to a relative increase in synaptic responses to 100-ms IPIs compared with 10-ms IPIs (Fig. 9*B*). It has been shown previously that IPI tuning first arises in the ELp and that ELa cells are tuned to EOD waveform but not IPI (21, 26). Since Hebbian STDP can alter the IPI tuning of ELp neurons, these results suggest that Hebbian STDP is acting on ELp-to-ELp synapses rather than on ELa-to-ELp synapses. In addition, we show that the peak of synaptic potential change for both sensory-leads-postsynaptic delays and postsynaptic-leads-sensory delays occurs >10 ms after stimulus onset (Fig. 6*A*). Previous work has shown that ELa response latencies to sensory stimuli are 2.5–3 ms (37) and ELp response latencies to sensory stimuli are 7–20 ms (43). Thus, the changes in synaptic potential in vivo occur in a time frame consistent with changes at ELp-to-ELp synapses. We also measured the onset slope of PSPs (Fig. 6, *B–D*). Previous work has shown that the onset slope of a PSP represents the immediate upstream presynaptic glutamate synapse (44), which in this case would be direct synapses from the ELa. We found no significant changes in onset slope following STDP, consistent with STDP acting at ELp-to-ELp synapses rather than ELa-to-ELp synapses. STDP acting at these synapses may also explain why ELp neurons with similar IPI tuning are more likely to share an excitatory synaptic connection, and why these excitatory synapses are stronger, compared with neurons with dissimilar IPI tuning (27).

Previous work has shown that STDP has a role in refining and altering responses to sensory input in vivo. In the passive and active electrosensory pathways of mormyrid fish, anti-Hebbian plasticity creates an efference copy, or "negative image," of predictable electrosensory input to cancel reafferent responses to self-generated input (12, 45). This anti-Hebbian plasticity occurs at the synapses between granule cells and medium ganglion cells, and individual granule cells have temporally diverse responses to self-generated input, allowing for a temporally specific efference copy (46). This cancellation generalizes across EOD rates through EOD command rate-dependent responses of granule cells and granule cell afferents (47). In the functionally similar cerebellum-like dorsal cochlear nucleus (DCN) of mice, synapses from parallel fibers onto fusiform and cartwheel cells exhibit Hebbian and anti-Hebbian STDP, respectively (48, 49). More recently, cancellation of self-generated reafferent auditory input in cartwheel cells has been shown to arise through a similar plastic efference copy that is generated through anti-Hebbian STDP (50). Both of these results are clear evidence that points to an important role for STDP in sensory processing. However, these findings show a role for STDP in the adaptive filtering of self-generated reafferent sensory input. Here, we wanted to address whether STDP could play a role in altering the sensory processing of externally generated, behaviorally relevant stimuli.

In the *Xenopus* tadpole visual system, Hebbian STDP evoked by moving bars occurs at retinotectal synapses in

vivo, leading to the development of motion direction tuning (14, 51, 52). Although this is clear evidence for Hebbian STDP altering sensory processing of external stimuli, these landmark studies occurred in developing juveniles, and we were interested in sensory processing in established adult circuits. In the locust olfactory system, small assemblies of Kenyon cells encode odor. Kenyon cells synapse onto β-lobe neurons, whose synchronous activity is required for fine odor discrimination (53). Hebbian STDP due to odor-evoked activity in Kenyon cells and β-lobe neuron synapses helps maintain the spiking synchrony required for feedforward information flow (54). In hippocampal place cells, STDP is likely involved in several processes related to spatial learning and may explain the anticipatory shifting of place fields due to experience (55). These studies have explored a role for STDP in sensory processing of adult circuits, but they have shown that STDP functions to maintain or reinforce an existing sensory representation rather than using STDP to modify responses to an actively changing sensory environment.

Multipolar cells exhibit the same IPI tuning to sensory stimulation as they do to direct electrical stimulation of ELa (26). This allows us to stimulate ELp in vivo and in vitro with the exact same temporal patterns (26, 27, 30, 31, 34). It follows that tuning in the ELp could be shifted via STDP in a similar way in vitro and in vivo. Despite this, although induction of STDP with presynaptic ELa focal stimulation in vitro (Fig. 2) resulted in clear synaptic plasticity and shifts in IPI tuning consistent with Hebbian STDP (Fig. 9*B*), we did not find such clear results when using array ELa stimulation in vitro or sensory stimulation in vivo (Fig. 5). Rather, we found that using presynaptic array stimulation or sensory stimulation paired with postsynaptic spiking could result in either potentiation or depression for pre-post delays close to zero rather than either/or as predicted by Hebbian STDP.

Recently, Chindemi et al. (56) showed that modeling long-term potentiation (LTP)/long-term depression (LTD) in pyramidal cells in the neocortex based on in vitro stimulation protocols created stereotypical potentiation and depression as expected, but when the model was adjusted for physiological levels of calcium LTP/LTD magnitudes were greatly reduced and required higher frequency stimulation to achieve. Further experiments manipulating the calcium concentration or stimulation frequency in vivo could be done to further elucidate what could be contributing to the discrepancy between our in vivo results and in vitro focal stimulation results. Alternative types of plasticity could also be involved. For example, the presence of synaptic clustering through cooperative plasticity allows for local plasticity in a group of functionally similar neurons (57–59). A well-studied mechanism in the field of memory formation (60), the consequence of this cooperative plasticity would be an anatomically restrained plasticity, where only synapses close enough together on the postsynaptic dendrite would be potentiated by repeated activation (57). Considering the dense interconnections and distinct tuning properties of ELp multipolar cells (27), it is possible that distinct clusters of synapses with different tuning properties and a differing presence of inhibition would all be affected by repeated stimulation variably.

In our system, previous work in the ELa has shown that a given EOD stimulates a unique population of ELa neurons (21, 25) and that ELa provides topographic, excitatory input to ELp (24). In addition, local excitatory connections between ELp multipolar cells are more common at short distances (27). Thus, focal ELa stimulation in vitro would drive activity in primarily local excitatory synapses between ELp neurons, in the topographic location corresponding to the ELa stimulation. In addition to excitatory input from ELa projection neurons and other ELp multipolar cells, multipolar cells also receive GABAergic inhibition from local interneurons (31). Array stimulation in vitro and sensory stimulation in vivo, however, would stimulate a more diffuse population of ELa projection neurons, driving postsynaptic activity in multipolar cells across the ELp, including more inhibitory pathways leading to the recorded neuron than expected from focal ELa stimulation. A stereotypically potentiating delay of pre-leads-postsynaptic activity could lead to visible depression in the postsynaptic response if the balance between excitatory and inhibitory pathways to the neuron was shifted relatively toward inhibitory pathways. If these inhibitory pathways were more numerous or more affected by STDP, this would result in STDP in the opposite of the predicted direction.

To begin to address this hypothesis, we performed a landmark calculation and PCA analysis on the in vitro array and in vivo data to determine whether physiological characteristics of synaptic responses correlated with variation in the direction of synaptic potential change induced by STDP. We found that there were significant differences in the PC scores depending on the "fit" of the data, i.e., whether or not the data followed the predicted direction of STDP (Figs. 7 and 10). Importantly, the PC scores reflected measures suggestive of differences in the balance of excitation and inhibition, among other things, in an individual PSP. These results suggest that more inhibition and polysynaptic activity could lead to a more diverse STDP response with array stimulation in vitro and sensory stimulation in vivo compared with focal stimulation in vitro, as both excitatory and inhibitory synapses could be under the influence of STDP.

Although induction of STDP with presynaptic ELa focal stimulation in vitro generates shifts in IPI tuning consistent with Hebbian STDP (Fig. 9*B*), we did not find such clear results when pairing postsynaptic spiking with specific IPIs in vivo. Though we did successfully induce statistically significant synaptic change in vivo in the direction predicted by Hebbian STDP (Fig. 5*D*), we found no significant shifts in EOD or IPI tuning (Figs. 8 and 9). Despite previous work showing the relevance of STDP in sensory processing, this disparity between in vitro and in vivo results highlights the large increase in variables that are contributing to plasticity and altering synaptic responses in vivo relative to in vitro. In conclusion, STDP is likely a relevant mechanism for shaping sensory processing, but its effects on responses to behaviorally relevant stimuli in intact organisms can be more complex than predicted by plasticity at specific synapses.

DATA AVAILABILITY

Data will be made available upon reasonable request.

SUPPLEMENTAL MATERIALS

Supplemental Figs. S1–S3 and Supplemental Tables S1–S4: https://doi.org/10.6084/m9.figshare.c.6339569.v2.

ACKNOWLEDGMENTS

We thank Matasaburo Fukutomi, Erika Schumacher, Martin Jarzyna, and Ellen Urquhart for general feedback and help with statistical analysis.

GRANTS

This work was supported by the National Science Foundation to B. A. Carlson, Grant IOS-1755071.

DISCLOSURES

No conflicts of interest, financial or otherwise, are declared by the authors.

AUTHOR CONTRIBUTIONS

A.J.L. and B.A.C. conceived and designed research; A.J.L. and X.M. performed experiments; A.J.L. and X.M. analyzed data; A.J.L. and B.A.C. interpreted results of experiments; A.J.L. prepared figures; A.J.L. drafted manuscript; A.J.L. and B.A.C. edited and revised manuscript; A.J.L., X.M., and B.A.C. approved final version of manuscript.

REFERENCES

1. **Sharpee TO**, **Calhoun AJ**, **Chalasani SH.** Information theory of adaptation in neurons, behavior, and mood. *Curr Opin Neurobiol* 25: 47–53, 2014. doi:10.1016/j.conb.2013.11.007.
2. **Wark B**, **Lundstrom BN**, **Fairhall A.** Sensory adaptation. *Curr Opin Neurobiol* 17: 423–429, 2007. doi:10.1016/j.conb.2007.07.001.
3. **Smirnakis SM**, **Berry MJ**, **Warland DK**, **Bialek W**, **Meister M.** Adaptation of retinal processing to image contrast and spatial scale. *Nature* 386: 69–73, 1997. doi:10.1038/386069a0.
4. **Dean I**, **Harper NS**, **McAlpine D.** Neural population coding of sound level adapts to stimulus statistics. *Nat Neurosci* 8: 1684–1689, 2005. doi:10.1038/nn1541.
5. **Chacron MJ**, **Doiron B**, **Maler L**, **Longtin A**, **Bastian J.** Non-classical receptive field mediates switch in a sensory neuron's frequency tuning. *Nature* 423: 77–81, 2003. [Erratum in Nature 424: 1018, 2003]. doi:10.1038/nature01590.
6. **Simoncelli EP**, **Olshausen BA.** Natural image statistics and neural representation. *Annu Rev Neurosci* 24: 1193–1216, 2001. doi:10.1146/annurev.neuro.24.1.1193.
7. **Solomon SG**, **Kohn A.** Moving sensory adaptation beyond suppressive effects in single neurons. *Curr Biol* 24: R1012–R1022, 2014. doi:10.1016/j.cub.2014.09.001.
8. **Whitmire CJ**, **Stanley GB.** Rapid sensory adaptation redux: a circuit perspective. *Neuron* 92: 298–315, 2016. doi:10.1016/j.neuron.2016.09.046.
9. **Dan Y**, **Poo M.** Spike timing-dependent plasticity of neural circuits. *Neuron* 44: 23–30, 2004. doi:10.1016/j.neuron.2004.09.007.
10. **Markram H**, **Lübke J**, **Frotscher M**, **Sakmann B.** Regulation of synaptic efficacy by coincidence of postsynaptic APs and EPSPs. *Science* 275: 213–215, 1997. doi:10.1126/science.275.5297.213.
11. **Feldman DE.** The spike-timing dependence of plasticity. *Neuron* 75: 556–571, 2012. doi:10.1016/j.neuron.2012.08.001.
12. **Bell CC**, **Han VZ**, **Sugawara Y**, **Grant K.** Synaptic plasticity in a cerebellum-like structure depends on temporal order. *Nature* 387: 278–281, 1997. doi:10.1038/387278a0.
13. **Bi GQ**, **Poo MM.** Synaptic modifications in cultured hippocampal neurons: dependence on spike timing, synaptic strength, and postsynaptic cell type. *J Neurosci* 18: 10464–10472, 1998. doi:10.1523/JNEUROSCI.18-24-10464.1998.
14. **Mu Y**, **Poo M.** Spike timing-dependent LTP/LTD mediates visual experience-dependent plasticity in a developing retinotectal system. *Neuron* 50: 115–125, 2006. doi:10.1016/j.neuron.2006.03.009.
15. **Richards BA**, **Aizenman CD**, **Akerman CJ.** In vivo spike-timing-dependent plasticity in the optic tectum of *Xenopus laevis*. *Front Synaptic Neurosci* 2: 7, 2010. doi:10.3389/fnsyn.2010.00007.
16. **Masquelier T**, **Thorpe SJ.** Unsupervised learning of visual features through spike timing dependent plasticity. *PLoS Comput Biol* 3: e31, 2007. doi:10.1371/journal.pcbi.0030031.
17. **Arai N**, **Müller-Dahlhaus F**, **Murakami T**, **Bliem B**, **Lu MK**, **Ugawa Y**, **Ziemann U.** State-dependent and timing-dependent bidirectional associative plasticity in the human SMA-M1 network. *J Neurosci* 31: 15376–15383, 2011. doi:10.1523/JNEUROSCI.2271-11.2011.
18. **Casula EP**, **Pellicciari MC**, **Picazio S**, **Caltagirone C**, **Koch G.** Spike-timing-dependent plasticity in the human dorso-lateral prefrontal cortex. *NeuroImage* 143: 204–213, 2016. doi:10.1016/j.neuroimage.2016.08.060.
19. **Testa-Silva G**, **Verhoog MB**, **Goriounova NA**, **Loebel A**, **Hjorth J**, **Baayen JC**, **de Kock CP**, **Mansvelder HD.** Human synapses show a wide temporal window for spike-timing-dependent plasticity. *Front Synaptic Neurosci* 2: 12, 2010. doi:10.3389/fnsyn.2010.00012.
20. **Carlson BA.** Electric signaling behavior and the mechanisms of electric organ discharge production in mormyrid fish. *J Physiol Paris* 96: 405–419, 2002. doi:10.1016/S0928-4257(03)00019-6.
21. **Baker CA**, **Kohashi T**, **Lyons-Warren AM**, **Ma X**, **Carlson BA.** Multiplexed temporal coding of electric communication signals in mormyrid fishes. *J Exp Biol* 216: 2365–2379, 2013. doi:10.1242/jeb.082289.
22. **Xu-Friedman MA**, **Hopkins CD.** Central mechanisms of temporal analysis in the knollenorgan pathway of mormyrid electric fish. *J Exp Biol* 202: 1311–1318, 1999. doi:10.1242/jeb.202.10.1311.
23. **Bell CC**, **Grant K.** Corollary discharge inhibition and preservation of temporal information in a sensory nucleus of mormyrid electric fish. *J Neurosci* 9: 1029–1044, 1989. doi:10.1523/JNEUROSCI.09-03-01029.1989.
24. **Friedman MA**, **Hopkins CD.** Neural substrates for species recognition in the time-coding electrosensory pathway of mormyrid electric fish. *J Neurosci* 18: 1171–1185, 1998. doi:10.1523/JNEUROSCI.18-03-01171.1998.
25. **Lyons-Warren AM**, **Kohashi T**, **Mennerick S**, **Carlson BA.** Detection of submillisecond spike timing differences based on delay-line anticoincidence detection. *J Neurophysiol* 110: 2295–2311, 2013. doi:10.1152/jn.00444.2013.
26. **Carlson BA.** Temporal-pattern recognition by single neurons in a sensory pathway devoted to social communication behavior. *J Neurosci* 29: 9417–9428, 2009. doi:10.1523/JNEUROSCI.1980-09.2009.
27. **Ma X**, **Kohashi T**, **Carlson BA.** Extensive excitatory network interactions shape temporal processing of communication signals in a model sensory system. *J Neurophysiol* 110: 456–469, 2013. doi:10.1152/jn.00145.2013.
28. **Carlson BA**, **Hasan SM**, **Hollmann M**, **Miller DB**, **Harmon LJ**, **Arnegard ME.** Brain evolution triggers increased diversification of electric fishes. *Science* 332: 583–586, 2011. doi:10.1126/science.1201524.
29. **Vélez A**, **Kohashi T**, **Lu A**, **Carlson BA.** The cellular and circuit basis for evolutionary change in sensory perception in mormyrid fishes. *Sci Rep* 7: 3783, 2017. doi:10.1038/s41598-017-03951-y.
30. **Kohashi T**, **Carlson BA.** A fast BK-type KCa current acts as a postsynaptic modulator of temporal selectivity for communication signals. *Front Cell Neurosci* 8: 286, 2014. doi:10.3389/fncel.2014.00286.
31. **George AA**, **Lyons-Warren AM**, **Ma X**, **Carlson BA.** A diversity of synaptic filters are created by temporal summation of excitation and inhibition. *J Neurosci* 31: 14721–14734, 2011. doi:10.1523/JNEUROSCI.1424-11.2011.
32. **Lyons-Warren AM**, **Kohashi T**, **Mennerick S**, **Carlson BA.** Retrograde fluorescent labeling allows for targeted extracellular single-unit recording from identified neurons in vivo. *J Vis Exp* 2013: 3921, 2013. doi:10.3791/3921.
33. **Baker CA**, **Ma L**, **Casareale CR**, **Carlson BA.** Behavioral and single-neuron sensitivity to millisecond variations in temporally patterned communication signals. *J Neurosci* 36: 8985–9000, 2016. doi:10.1523/JNEUROSCI.0648-16.2016.
34. **Baker CA**, **Carlson BA.** Short-term depression, temporal summation, and onset inhibition shape interval tuning in midbrain neurons. *J Neurosci* 34: 14272–14287, 2014. doi:10.1523/JNEUROSCI.2299-14.2014.
35. **Rose G**, **Fortune E.** New techniques for making whole-cell recordings from CNS neurons in vivo. *Neurosci Res* 26: 89–94, 1996. doi:10.1016/0168-0102(96)01074-7.

36. **Yoder N.** peakfinder(x0, sel, thresh, extrema, includeEndpoints, interpolate) (Online). https://www.mathworks.com/matlabcentral/fileexchange/25500-peakfinder-x0-sel-thresh-extrema-includeendpoints-interpolate [2021 Nov 17].
37. **Amagai S**, **Friedman MA**, **Hopkins CD.** Time coding in the midbrain of mormyrid electric fish. I. Physiology and anatomy of cells in the nucleus exterolateralis pars anterior. *J Comp Physiol A* 182: 115–130, 1998. doi:10.1007/s003590050163.
38. **Hopkins CD**, **Bass AH.** Temporal coding of species recognition signals in an electric fish. *Science* 212: 85–87, 1981. doi:10.1126/science.7209524.
39. **Markram H**, **Lübke J**, **Frotscher M**, **Roth A**, **Sakmann B.** Physiology and anatomy of synaptic connections between thick tufted pyramidal neurones in the developing rat neocortex. *J Physiol* 500: 409–440, 1997. doi:10.1113/jphysiol.1997.sp022031.
40. **Song S**, **Miller KD**, **Abbott LF.** Competitive Hebbian learning through spike-timing-dependent synaptic plasticity. *Nat Neurosci* 3: 919–926, 2000. doi:10.1038/78829.
41. **Morrison A**, **Diesmann M**, **Gerstner W.** Phenomenological models of synaptic plasticity based on spike timing. *Biol Cybern* 98: 459–478, 2008. doi:10.1007/s00422-008-0233-1.
42. **Huang QS**, **Wei H.** A computational model of working memory based on spike-timing-dependent plasticity. *Front Comput Neurosci* 15: 630999, 2021. doi:10.3389/fncom.2021.630999.
43. **Amagai S.** Time coding in the midbrain of mormyrid electric fish. II. Stimulus selectivity in the nucleus exterolateralis pars posterior. *J Comp Physiol A* 182: 131–143, 1998. doi:10.1007/s003590050164.
44. **Taube JS**, **Schwartzkroin PA.** Mechanisms of long-term potentiation: EPSP/spike dissociation, intradendritic recordings, and glutamate sensitivity. *J Neurosci* 8: 1632–1644, 1988. doi:10.1523/JNEUROSCI.08-05-01632.1988.
45. **Warren R**, **Sawtell NB.** A comparative approach to cerebellar function: insights from electrosensory systems. *Curr Opin Neurobiol* 41: 31–37, 2016. doi:10.1016/j.conb.2016.07.012.
46. **Kennedy A**, **Wayne G**, **Kaifosh P**, **Alviña K**, **Abbott LF**, **Sawtell NB.** A temporal basis for predicting the sensory consequences of motor commands in an electric fish. *Nat Neurosci* 17: 416–422, 2014. doi:10.1038/nn.3650.
47. **Dempsey C**, **Abbott LF**, **Sawtell NB.** Generalization of learned responses in the mormyrid electrosensory lobe. *eLife* 8: e44032, 2019. doi:10.7554/eLife.44032.
48. **Fujino K**, **Oertel D.** Bidirectional synaptic plasticity in the cerebellum-like mammalian dorsal cochlear nucleus. *Proc Natl Acad Sci USA* 100: 265–270, 2003. doi:10.1073/pnas.0135345100.
49. **Tzounopoulos T**, **Kim Y**, **Oertel D**, **Trussell LO.** Cell-specific, spike timing-dependent plasticities in the dorsal cochlear nucleus. *Nat Neurosci* 7: 719–725, 2004. doi:10.1038/nn1272.
50. **Singla S**, **Dempsey C**, **Warren R**, **Enikolopov AG**, **Sawtell NB.** A cerebellum-like circuit in the auditory system cancels responses to self-generated sounds. *Nat Neurosci* 20: 943–950, 2017. doi:10.1038/nn.4567.
51. **Zhang LI**, **Tao HW**, **Holt CE**, **Harris WA**, **Poo M.** A critical window for cooperation and competition among developing retinotectal synapses. *Nature* 395: 37–44, 1998. doi:10.1038/25665.
52. **Engert F**, **Tao HW**, **Zhang LI**, **Poo M.** Moving visual stimuli rapidly induce direction sensitivity of developing tectal neurons. *Nature* 419: 470–475, 2002. doi:10.1038/nature00988.
53. **MacLeod K**, **Bäcker A**, **Laurent G.** Who reads temporal information contained across synchronized and oscillatory spike trains? *Nature* 395: 693–698, 1998. doi:10.1038/27201.
54. **Cassenaer S**, **Laurent G.** Hebbian STDP in mushroom bodies facilitates the synchronous flow of olfactory information in locusts. *Nature* 448: 709–713, 2007. doi:10.1038/nature05973.
55. **Mehta MR.** From synaptic plasticity to spatial maps and sequence learning: place field plasticity. *Hippocampus* 25: 756–762, 2015. [Erratum in *Hippocampus* 25: 771, 2015]. doi:10.1002/hipo.22472.
56. **Chindemi G**, **Abdellah M**, **Amsalem O**, **Benavides-Piccione R**, **Delattre V**, **Doron M**, **Ecker A**, **Jaquier AT**, **King J**, **Kumbhar P**, **Monney C**, **Perin R**, **Rössert C**, **Tuncel AM**, **Van Geit W**, **DeFelipe J**, **Graupner M**, **Segev I**, **Markram H**, **Muller EB.** A calcium-based plasticity model for predicting long-term potentiation and depression in the neocortex. *Nat Commun* 13: 3038, 2022. doi:10.1038/s41467-022-30214-w.
57. **Mehta MR.** Cooperative LTP can map memory sequences on dendritic branches. *Trends Neurosci* 27: 69–72, 2004. doi:10.1016/j.tins.2003.12.004.
58. **Harvey CD**, **Svoboda K.** Locally dynamic synaptic learning rules in pyramidal neuron dendrites. *Nature* 450: 1195–1200, 2007. doi:10.1038/nature06416.
59. **Larkum ME**, **Nevian T.** Synaptic clustering by dendritic signalling mechanisms. *Curr Opin Neurobiol* 18: 321–331, 2008. doi:10.1016/j.conb.2008.08.013.
60. **Kastellakis G**, **Poirazi P.** Synaptic clustering and memory formation. *Front Mol Neurosci* 12: 300, 2019. doi:10.3389/fnmol.2019.00300. .